Cross-Coupling Mitigation in Polarimetric PAR via Antenna Tilt

IGOR R. IVIĆ[a,b]

[a] *Cooperative Institute for Severe and High-Impact Weather Research and Operations, University of Oklahoma, Norman, Oklahoma*
[b] *NOAA/OAR/National Severe Storms Laboratory, Norman, Oklahoma*

(Manuscript received 6 June 2022, in final form 4 February 2023, accepted 2 March 2023)

ABSTRACT: The existence of significant cross-polar antenna patterns, as well as the scan-dependent measurement biases, inherent to the polarimetric phased array radar (PPAR), are among the most important risk factors for using this technology in weather observations. The cross-polar patterns on receive induce cross coupling between returns from the two orthogonal fields causing biases in polarimetric variable estimates. Furthermore, the electromagnetic coupling in hardware may exacerbate the cross-coupling effects. To address this problem, a pulse-to-pulse phase coding in either the horizontal or vertical ports of the transmission elements has been proposed. However, it does not affect the scan-dependent system biases in PPAR estimates, which require corrections via calibration mechanisms. Further, the cross-coupling signals are proportional to the cross-polar pattern power levels, rendering mitigation effective only at steering angles where these levels are sufficiently low (e.g., approximately less than −25 dB). In that regard, any approach that augments the number of such steering angles benefits the cross-coupling mitigation effectiveness. Herein, a simple approach that has a potential to achieve this via antenna tilt is presented.

SIGNIFICANCE STATEMENT: The issue of biases caused by cross coupling (due to significant cross-polar patterns in PPARs) is one of the biggest challenges for their weather observation applications. Numerous approaches have been proposed to address this issue, but none has been comprehensive. This suggests that the solution to the cross-coupling issue should be a combination of various mitigation approaches. In that regard, it is suggested in this work that a small antenna tilt can aid in the mitigation of the cross-coupling issue.

KEYWORDS: Radars/Radar observations; Remote sensing; Weather radar signal processing

1. Introduction

One of the main requirements for the improvement of weather observations using ground-based Doppler radars in the United States is high-temporal-resolution data [e.g., on the order of ~1 min as opposed to the ~5 min currently provided by the Weather Surveillance Radar-1988 Doppler (WSR-88D) network] (Crum and Alberty 1993). The phased array radar (PAR) technology supports more flexible scanning strategies than radars with mechanically steered antennas and is expected to ultimately reduce data update times (Zrnić et al. 2007; Heinselman and Torres 2011; Torres et al. 2016; Weber 2019). Thus, one option for the development of improved weather surveillance systems is the adoption of PAR technology for weather applications (Zrnić et al. 2007; Weber et al. 2021). Concurrently, the dual-polarization capability (Zrnić and Ryzhkov 1999) has become standard for parabolic-antenna radars used for weather observations and is one of the essential requirements for the future weather radar network. In turn, this requirement imposes the need for a strict calibration of a polarimetric PAR (PPAR) to achieve measurement accuracies of well-calibrated parabolic-antenna-based weather radar.

The weather-derived products which drive the requirements for the accuracy of polarimetric measurements are differential reflectivity (Z_{DR}), copolar correlation coefficient ($|\rho_{hv}|$), and specific differential phase (K_{DP}) (Doviak and Zrnić 1993; Bringi and Chandrasekar 2001); Z_{DR} is defined as the logarithm of the horizontal (H) to vertical (V) returned powers ratio, ρ_{hv} is the correlation coefficient between H and V returns, and K_{DP} is the derivative of the differential phase (ϕ_{DP}) with respect to range, where ϕ_{DP} is the phase difference between the returns in H and V (Doviak and Zrnić 1993) at a given scanning direction and range. To conduct precise measurements of polarimetric variables, the radar should transmit linearly polarized H and V fields through beams well-matched in gain and shape at every scanning direction. On reception, the gains, as well as shapes of H and V antenna radiation patterns, must also be well matched with ideally no cross coupling between the two orthogonal polarization channels. Such characteristics are difficult to achieve because polarization, shape, and gain of radiation patterns in current phased-array antennas inherently depend on the beam-pointing direction (i.e., electronic steering angle). As an example, arrays of patch antenna elements (common because of their low cost and relative manufacturing ease) produce orthogonal H and V fields only in the principal planes of the array, whereas the radiated fields increasingly depart from their intended orientations in other directions. This results in the rising levels of cross-polar patterns on transmit and receive as beams are electronically steered away from principal planes. Furthermore, due to the proximity of hardware in a PPAR, inductive and/or capacitive coupling can cause leakage of the energy present in the H channel into the V channel, and vice versa (herein referred to as the hardware cross coupling). The presence of these effects induces cross coupling of the H and V returns causing

Corresponding author: Igor R. Ivić, igor.ivic@noaa.gov

DOI: 10.1175/JTECH-D-22-0059.1

significant biases (i.e., cross-coupling biases) in the estimates of polarimetric variables (Wang and Chandrasekar 2006; Zrnić et al. 2010).

To achieve an accurate estimation of rainfall rates, it is recommended that the bias of Z_{DR} estimates (i.e., $\hat{Z}_{DR}$, where the caret denotes the estimate) is kept within ±0.1 dB for intrinsic (i.e., true) Z_{DR} between 0 and 1 dB and less than $0.1 \times Z_{DR}$ for larger Z_{DR} values (Zrnić et al. 2010). This imposes a strict requirement of more than 50 dB of isolation between the H and V signals in the antenna hardware (Zrnić et al. 2012; Ivić and Doviak 2016; Ivić 2022). It should be noted that keeping the bias of Z_{DR} estimates within ±0.1 dB is exceptionally difficult to achieve even in radars with parabolic antennas (e.g., on the WSR-88D network; Richardson et al. 2017), and for this reason the bias accuracy within ±0.2 dB for Z_{DR} less than 1 dB (and up to $0.2 \times Z_{DR}$ for larger Z_{DR} values) seems more feasible at this time. In the case of $|\rho_{hv}|$ estimates ($|\hat{\rho}_{hv}|$), a bias within ±0.01 is deemed sufficient for "sensing the mixed-phase precipitation and gauging the hail size quantitatively" (Balakrishnan and Zrnić 1990). NOAA/NWS radar functional requirements (RFR; NOAA/NWS 2015), however, set the bias limits for $|\rho_{hv}|$ estimates to an even more stringent value of ±0.006. For $\hat{\phi}_{DP}$, NOAA/NWS RFR bias limit requirements are ±1°.

Multiple approaches to address the cross-coupling issue have been proposed. These range from cylindrical antenna configurations or cylindrical PPAR (CPPAR) (Zhang et al. 2011; Josefsson and Persson 2006; Karimkashi and Zhang 2015; Fulton et al. 2017) whereby beams are typically always scanned along the vertical principal plane, to those that mitigate the cross coupling in planar antennas (Crain and Staiman 2007; Galletti et al. 2014; Leifer et al. 2013; Zrnić et al. 2014; Pidre et al. 2017). These are summarized in Ivić and Doviak (2016). In the case of a planar PPAR antenna, a maximum range of steering angles used in a configuration affects the cross-coupling mitigation requirements. For instance, a four-faced PPAR where each face electronically scans a 90° sector presents the most challenge. This is because the cross-coupling increases radically as electronic steering considerably departs from the principal planes. If a single-face rotating PPAR is used (Schvartzman 2020), the scanning directions would be typically constrained to the vicinity of principal planes where the cross coupling is usually small. In such a case, however, "multiple digitally formed receive beams, complemented by adaptive scanning and dwell-time reduction where appropriate would be required" (Weber 2019; Schvartzman et al. 2021b,a, 2022). It should be noted, though, that scanning a 90° sector with stationary antenna may be a requirement even with a single-face rotating PPAR in particular situations. These may include, but are not limited to, a rapid scanning of a 90° sector that is of particular interest using range–height indicator (RHI) or plan position indicator (PPI) scanning strategies.

In addition to cross coupling, the variable (with beam steering angle) array impedances, as well as differences in the gains and shapes between H and V copolar patterns, may cause variable system Z_{DR} and ϕ_{DP} biases at every boresight direction. The aforementioned approaches do not correct this bias (i.e., the copolar bias), so it must be accounted for using a separate calibration mechanism to produce correction values that can be used in the signal processing stage (Ivić et al. 2021). Such a mechanism must characterize copolar antenna patterns at and around main beam peaks with sufficient accuracy. It also requires calibration measurements at potentially regular time intervals to account for possible system variabilities. Unless cross-coupling mitigations and copolar calibration corrections are successfully applied, these effects have a profound adverse impact on the quality of polarimetric measurements needed to identify different types of hydrometeors and estimate precipitation rates accurately.

Dual polarization can be implemented by either alternately or simultaneously exciting the H and V ports of the antenna while receiving H and V echoes simultaneously. The first implementation is known as the alternating transmit simultaneous receive (ATSR) and the second as the simultaneous transmit simultaneous receive (STSR) (Doviak et al. 2000). Because the WSR-88Ds use the latter (Doviak et al. 2000; Melnikov and Zrnić 2015), the STSR mode is the preferred mode of operation for PPAR systems aiming to replace the current WSR-88Ds (whereby the STSR mode has been chosen for implementation on the WSR-88D fleet because of advantages in reducing errors of estimates while mitigating the effects of range–velocity ambiguities; Melnikov and Zrnić 2015). This would allow the current WSR-88D algorithms, developed for the STSR mode [e.g., range and velocity ambiguity mitigation techniques (Sirmans et al. 1976; Zrnić and Mahapatra 1985; Sachidananda and Zrnić 1999), as well as frequency clutter filtering using GMAP (Siggia and Passarelli 2004) or CLEAN-AP (Torres and Warde 2014) filters], to be used by the PPARs. However, this further complicates polarimetric observations via PPAR because the STSR mode is more susceptible to the effects of cross coupling than the ATSR mode (Zrnić et al. 2012).

Stagliano and Holder (2010) proposed the use of orthogonal phase codes on transmit (without recommending the specific code sequence) to improve the cross-polar isolation in the STSR mode (thus mitigating Z_{DR} bias caused by cross coupling). Subsequently, Leifer et al. (2013) suggested the use of orthogonal Walsh–Hadamard phase codes [also proposed in Chandrasekar and Bharadwaj (2009) for simultaneous co- and cross-polarization measurements in the STSR mode] on the transmitted H and V polarized pulse trains (i.e., pulse-to-pulse phase coding). Around the same time, the use of the alternating pulse-to-pulse 180° phase shifts (a subset of the Walsh–Hadamard codes) was proposed by Zrnić et al. (2014) without presenting a comprehensive statistical evaluation in terms of bias and the standard deviation. The latter was given in Ivić and Doviak (2016), while the effects on Doppler spectra are described in Ivić (2018b). An experimental demonstration and evaluation of the technique is presented in Ivić (2022). This mode is referred to as the phase-coded STSR (PCSTSR) mode. Assuming the presence of a unimodal weather signal, the cited works demonstrate the significant mitigation of $\hat{Z}_{DR}$ bias introduced by cross-polar patterns using time-domain signal processing (i.e., pulse-pair processing; Doviak and Zrnić 1993). This greatly increases the scan area where the effects of cross coupling can be neglected and only the copolar bias must be corrected. In the best case, this method may reduce the cross-coupling

biases of Z_{DR} and ϕ_{DP} estimates to those obtained in the ATSR mode. In the case of $|\hat{\rho}_{hv}|$, however, it was found that the application of phase coding induces negative bias in the estimates of $|\rho_{hv}|$ (Ivić 2017), but it can be mitigated via filtering in spectral domain (Ivić 2022). In summary, the strong cross-polar patterns will likely produce biases beyond the required limits at boresight locations far away from principal planes (as indicated in Ivić 2017).

In addition to the pulse-to-pulse phase coding, another approach has been proposed by Zrnić et al. (2014) for mitigation of the cross-coupling effects. It is based on time multiplexing approach, whereby the V transmitter port is energized immediately after the H port or vice versa. This results in transmitted H and V pulses that are shifted by one pulse width relative to each other. Further investigation of this approach (Ivić 2016) indicates that the efficacy of this approach is diminished by reflectivity gradients in range and antenna gain mismatches. This designates pulse-to-pulse phase coding as the preferable option for cross-coupling mitigation.

For boresight locations where the cross-coupling mitigation in the PCSTSR mode is insufficient, a full correction may be applied using the knowledge of both the copolar and cross-polar patterns. Assuming the reciprocal radar antenna system (i.e., transmit and receive patterns are the same), such corrections are formulated in Zhang et al. (2009) and Zrnić et al. (2011), where each PPAR radiation element is treated as a pair of crossed Hertzian dipoles or idealized aperture as well as a patch in Lei at al. (2013). However, the reciprocity assumption is usually not valid for PPARs, which use active components (e.g., T/R modules). Also, real radiators are likely to behave differently than idealized ones (e.g., due to the mutual coupling among them as well as manufacturing imperfections). In Pang et al. (2016) and Fulton and Chappell (2010), bias corrections that make no assumptions about the radiating element are presented. The correction in the ATSR mode is proposed by Pang et al. (2016) and uses the knowledge of beam peaks (i.e., beam pattern values at boresight). A correction method applicable in the STSR mode is described in Fulton and Chappell (2010) along with experimental evaluation. It is demonstrated using a vertically polarized S-band subarray panel with 16 elements and element-level digitization on both transmit and receive. Corrections proposed in Pang et al. (2016) as well as Fulton and Chappell (2010) require separate manipulation of powers and phases of transmitter excitations (which must be performed in hardware) as well as computational manipulation of receive signals (which can be performed in hardware or software). An approach to a full correction that avoids hardware manipulations and can be implemented solely in the signal processing, but requires characterization of co- and cross-polar fields as in Pang et al. (2016) and Fulton and Chappell (2010), is proposed in Ivić (2018b).

It is clear that the estimates of polarimetric variables from PPAR data must be corrected using the knowledge of co- and cross-polar pattern main beams to achieve acceptable accuracies. Such knowledge may be acquired via sufficiently precise far-field and/or near-field measurements. Also, the use of computational electromagnetic (CEM) tools may be useful for exploring the behaviors of passive components (e.g., patch radiators) used in the construction of antenna hardware. At the current state of technology, however, it is unlikely that CEM can capture the effects of active components in the antenna backplane (e.g., T/R elements) which affect antenna patterns. Nevertheless, as PPAR technology improves the gap between CEM results and real PPAR behaviors may diminish and in that regard the limits of CEM have not yet been fully explored. If the cross-coupling biases are well below the prescribed limits, only the copolar bias needs to be corrected using the knowledge of copolar patterns at boresight locations of interest. In planar PPAR this may be the case only for a subset of boresight locations of interest. If a CPPAR configuration is used, the correction of copolar biases would be needed only for boresight locations in the vertical principal plane (Karimkashi and Zhang 2015; Fulton et al. 2017). It should be noted, though, that if significant hardware coupling is present, it increases cross coupling at all boresight locations (including principal planes). In that regard. the use of PCSTSR mode mitigates the effects of cross coupling in general (i.e., the cross coupling through both the antenna patterns and hardware) and increases the scan area where only the correction of copolar bias is needed to achieve the required accuracy. Such an approach is desirable because it circumvents the need to characterize the cross-polar patterns, at and around boresight, which are more difficult to measure with high accuracy than the copolar ones (since they are smaller in power). In that regard, it is beneficial to increase the number of boresight directions at which only correction for copolar bias is needed. Herein, the effects of the antenna tilt are examined to explore if these effects can be used to improve the overall polarimetric performance of a planar PPAR.

These effects have been studied by Orzel and Frasier (2018) in the case of an azimuth scanning array that must be mechanically tilted to scan in elevation. In this context, they based the derivation of polarization orientation dependence on the tilt and electronic scan angle on a pair of crossed dipoles. Real array radiator elements, however, typically exhibit the behavior that significantly departs from that of a pair of crossed dipoles. In that regard, an approach presented in this work makes no assumptions on the antenna pattern behavior but rather utilizes the prior knowledge of the antenna copolar and cross-polar patterns (e.g., from measurements or simulations). For this reason, a tilt matrix that maps the known radiation patterns relative to the antenna face plane to ground relative radiation is derived. It is used to compute the resultant tilted antenna copolar and cross-polar radiation, which impinges on hydrometeors, as well as to determine the received copolar and cross-polar radiation scattered back to the radar.

The paper is structured as follows. A theoretical analysis is presented in section 2 to provide an insight into the underlying framework used to produce the results described in section 3. Note that the framework described in section 2 relies on previous works as indicated in the text. The main conclusions of the paper are summarized in section 4.

2. Theoretical analysis

The analysis conducted herein assumes hydrometeors are oblate spheroids with a net mean canting angle close to zero

(Oguchi 1983). In such a case the effects of depolarization induced by hydrometeors are negligible because the sum of the backscattering matrix (Stapor and Pratt 1984) off-diagonal elements (i.e., s_{hv} and s_{vh}) across scatterers illuminated by the antenna radiation pattern within the range resolution cell is close to zero [i.e., $\sum_n s_{vh}(n) = \sum_n s_{vh}(n) \approx 0$]. Consequently, a generalization is introduced so that off-diagonal elements in the backscattering matrix of each scatterer are set to zero for analysis purposes. This reflects the fact that the only depolarization is that induced by the system when hydrometeors whose net mean canting angle is zero (i.e., nondepolarizing scatterers) are observed, (i.e., $s_{hv} = s_{vh} \approx 0$; Oguchi 1983; Stapor and Pratt 1984; Sachidananda and Zrnić 1985). The zero net mean canting angle assumption is valid for the majority of hydrometeors (e.g., rain) but not for all (Ryzhkov and Zrnić 2007; Illingworth and Thompson 2011). Nonetheless, the zero mean canting angle assumption is valid herein because this work aims to mitigate the adverse effects of the system depolarization, while the effects of depolarizing media are beyond the scope of this work.

Herein, a theoretical model using a subvolume approach, presented in Ivić and Doviak (2016), is assumed. In this model, signals received in H and V are viewed as the sums of differential voltages that describe returns from a large number of scatterers contained in subvolumes bound by the resolution of the antenna patterns in azimuth and elevation. For simplicity, the elements of the transmission matrix $\mathbf{T}$ [which describes the effects of precipitation along the propagation path and is given by Eq. (8.53) in Doviak and Zrnić (1993)] are merged into the elements of the backscattering matrix. In such a model, elements on the main diagonal of the backscattering matrix are

$$\begin{aligned} s_{hh}(m) &= \sum_n s_{hh}(n)\exp[-j2kr_n(m)]\exp(-j\phi_{DP}), \\ s_{vv}(m) &= \sum_n s_{vv}(n)\exp[-j2kr_n(m)], \end{aligned} \tag{1}$$

where m stands for the mth transmission and the sums are across n scatterers in a subvolume. Also, k is the wavenumber and $r_n(m)$ is the distance of each scatterer at the time of mth transmission.

Under these assumptions, the differential echo voltages produced by the returns from scatterers contained in a subvolume located at a given azimuth, elevation, and range illuminated by mth transmission are represented [by expanding on the rationale exemplified by Eq. (3) in Zrnić et al. (2010)] as

$$\begin{aligned} \begin{bmatrix} dV_h(m) \\ dV_v(m) \end{bmatrix} &= C\mathbf{R}_H\mathbf{F}_R\mathbf{T}_A^t\mathbf{S}\mathbf{T}_A\mathbf{F}_T\mathbf{T}_H\mathbf{E}_{hv}\mathbf{e} \\ &= C\begin{bmatrix} R_{hh}^H & R_{vh}^H \\ R_{hv}^H & R_{vv}^H \end{bmatrix}\begin{bmatrix} F_{rh}^{co} & F_{rh}^{x} \\ F_{rv}^{x} & F_{rv}^{co} \end{bmatrix}\begin{bmatrix} T_{11}^A & T_{21}^A \\ T_{12}^A & T_{22}^A \end{bmatrix} \\ &\times \begin{bmatrix} s_{hh}(m) & 0 \\ 0 & s_{vv}(m) \end{bmatrix} \times \begin{bmatrix} T_{11}^A & T_{12}^A \\ T_{21}^A & T_{22}^A \end{bmatrix} \\ &\times \begin{bmatrix} F_{th}^{co} & F_{tv}^{x} \\ F_{th}^{x} & F_{tv}^{co} \end{bmatrix}\begin{bmatrix} T_{hh}^H & T_{vh}^H \\ T_{hv}^H & T_{vv}^H \end{bmatrix}\begin{bmatrix} e_h & 0 \\ 0 & e_v \end{bmatrix} \\ &\times \begin{bmatrix} A_h(m)e^{j\alpha_h(m)} \\ A_v(m)e^{j\alpha_v(m)} \end{bmatrix}, \end{aligned} \tag{2}$$

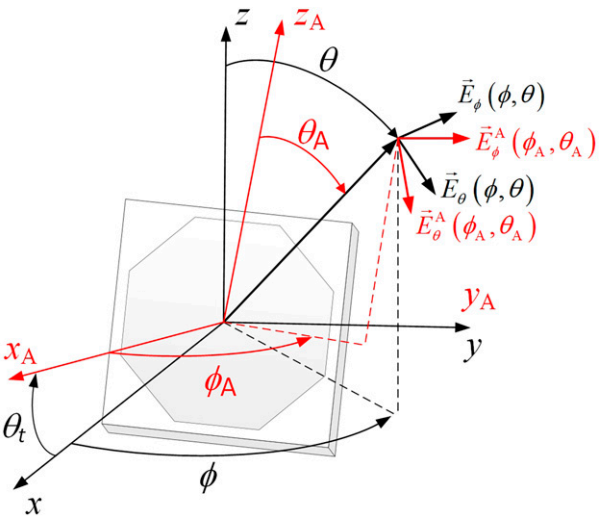

FIG. 1. A spherical coordinate system used to plot radiation patterns. The coordinate system shown in black is tied to the ground and the one in red is tied to the antenna.

where superscript "t" indicates the transposed matrix. In (2), elements of the intended excitation vector $\mathbf{e}$ are

$$\begin{aligned} &\text{STSR}: A_h(m) = A_v(m) = 1, \\ &\text{ATSR}: A_h(m) = \frac{1+(-1)^m}{2} \quad \text{and} \quad A_v(m) = \frac{1+(-1)^{m+1}}{2}, \end{aligned} \tag{3}$$

while $\alpha_h(m)$ and $\alpha_h(m)$ denote the phase shifts imposed on transmission in H and V to implement the pulse-to-pulse phase coding. The quantities e_h and e_v are complex numbers that describe the effects caused by variations of the array impedances as a function of scanning angle, which result in the actual excitations of H and V ports of unequal magnitude and phase. Symbols $\mathbf{F}_T$ and $\mathbf{F}_R$ denote the antenna pattern matrices on transmit and receive, respectively. The elements of $\mathbf{F}_T$ and $\mathbf{F}_R$ (i.e., F_{lp}^c, where l can be either "t" or "r," p is either "h" or "v," and c is either "co" or "x") are one-way electric field patterns that are complex functions of the boresight direction θ_0, ϕ_0 (Fig. 1). This dependency is imposed by the array factor (i.e., a directional two-dimensional function that weights the pattern shapes of individual radiators via controlling the relative phases and amplitudes of the radio waves emitted by the antenna elements in the array), the variable array impedances, the pattern shapes of individual radiators as well as mutual coupling among them. Note that this dependency does not exist in parabolic reflector antennas. Symbols F_{th}^{co} and F_{rh}^{co} denote the copolar patterns (i.e., polarization concomitant with $\mathbf{E}_\phi$ in Fig. 1) in H on transmit and receive, respectively. Similar definitions apply to F_{th}^{x} and F_{rh}^{x} for the cross-polar patterns (i.e., polarization concomitant with $\mathbf{E}_\theta$ in Fig. 1) in H. Analogously, F_{tv}^{co}, F_{rv}^{co}, F_{tv}^{x}, and F_{rv}^{x} denote the co- (i.e., polarization concomitant with $\mathbf{E}_\theta$ in Fig. 1) and cross-

polar patterns (i.e., polarization concomitant with $\mathbf{E}_\phi$ in Fig. 1) in V. These patterns are the result of the array passive components (e.g., patch elements) organized in a two-dimensional lattice to form an antenna. As such, these account for the radiator effects as well as the mutual couplings among them. Elements of matrices $\mathbf{T}_H$ and $\mathbf{R}_H$ are complex numbers that describe the mismatches and parasitic couplings between and among the active and passive antenna hardware on transmit and receive in the antenna backplane (e.g., T/R elements and cabling), respectively. Elements of $\mathbf{R}_H$ may also account for the attenuations and phase shifts in the H and V receiver paths. For simplicity, a high enough signal-to-noise ratio (SNR) is assumed so that the effects of noise can be neglected. Finally, C is a scalar factor that contains dependence on resolution volume range location, and system parameters.

Note that the $\mathbf{F}_T$, $\mathbf{T}_H$, and $\mathbf{E}_{hv}$, as well as $\mathbf{F}_R$ and $\mathbf{R}_H$, can be merged to produce

$$\mathbf{T}_S = \mathbf{F}_T\mathbf{T}_H\mathbf{E}_{hv} = \begin{bmatrix} T_h^{co} & T_v^{x} \\ T_h^{x} & T_v^{co} \end{bmatrix},$$

$$\mathbf{R}_S = \mathbf{R}_H\mathbf{F}_R = \begin{bmatrix} R_h^{co} & R_h^{x} \\ R_v^{x} & R_v^{co} \end{bmatrix}. \tag{4}$$

Matrices $\mathbf{T}_S$ and $\mathbf{R}_S$ represent the "cumulative" patterns that describe the cross coupling (via elements off the main diagonal) through both the antenna cross-polar patterns and hardware, as well as the excitation and the receive path effects. The matrix $\mathbf{T}_A$ accounts for the effects of antenna tilt relative to the ground (appendix). Thus, the patterns that include the effects of the antenna tilt can be obtained as

$$\begin{aligned} \mathbf{T}_{TS} &= \mathbf{T}_A\mathbf{T}_S = \begin{bmatrix} T_{th}^{co} & T_{tv}^{x} \\ T_{th}^{x} & T_{tv}^{co} \end{bmatrix} \\ &= \begin{bmatrix} T_{11}^A T_h^{co} + T_{12}^A T_h^{x} & T_{11}^A T_v^{x} + T_{12}^A T_v^{co} \\ T_{21}^A T_h^{co} + T_{22}^A T_h^{x} & T_{21}^A T_v^{x} + T_{22}^A T_v^{co} \end{bmatrix}, \\ \mathbf{R}_{TS} &= \mathbf{R}_S\mathbf{T}_A^t = \begin{bmatrix} R_{th}^{co} & R_{th}^{x} \\ R_{th}^{x} & R_{th}^{co} \end{bmatrix} \\ &= \begin{bmatrix} T_{11}^A R_h^{co} + T_{12}^A R_h^{x} & T_{21}^A R_h^{co} + T_{22}^A R_h^{x} \\ T_{11}^A R_v^{x} + T_{12}^A R_v^{co} & T_{21}^A R_v^{x} + T_{22}^A R_v^{co} \end{bmatrix}. \end{aligned} \tag{5}$$

From (5), it is obvious that the antenna tilt changes the apparent antenna patterns (i.e., the antenna patterns in the spherical coordinate system tied to the ground). Clearly, the cross-polar patterns are more affected by the tilt than the copolar ones. This is because the copolar pattern levels are significantly larger than those of the cross-polar patterns. Consequently, the addition of the small portion of a copolar pattern [weighted by the off-diagonal elements of the tilt matrix as shown in (5)] to the cross-polar one affects the latter significantly but not vice versa. In particular, the pattern powers at each ϕ and θ are (note that the elements of the tilt matrix are real numbers while the elements of the $\mathbf{T}_S$ and $\mathbf{R}_S$ matrices are complex numbers)

$$\begin{aligned} |C_{th}^{co}(\phi,\theta)|^2 &= |T_{11}^A C_h^{co}(\phi_A,\theta_A)|^2 + |T_{12}^A C_h^{x}(\phi_A,\theta_A)|^2 \\ &\quad + 2|T_{11}^A C_h^{co}(\phi_A,\theta_A) T_{12}^A C_h^{x}(\phi_A,\theta_A)| \\ &\quad \times \cos[\text{angle}\{T_{11}^A C_h^{co}(\phi_A,\theta_A)\} \\ &\quad - \text{angle}\{T_{12}^A C_h^{x}(\phi_A,\theta_A)\}], \\ |C_{th}^{x}(\phi,\theta)|^2 &= |T_{21}^A C_h^{co}(\phi_A,\theta_A)|^2 + |T_{22}^A C_h^{x}(\phi_A,\theta_A)|^2 \\ &\quad + 2|T_{21}^A C_h^{co}(\phi_A,\theta_A) T_{22}^A C_h^{x}(\phi_A,\theta_A)| \\ &\quad \times \cos[\text{angle}\{T_{21}^A C_h^{co}(\phi_A,\theta_A)\} \\ &\quad - \text{angle}\{T_{22}^A C_h^{x}(\phi_A,\theta_A)\}], \\ |C_{tv}^{co}(\phi,\theta)|^2 &= |T_{21}^A C_v^{x}(\phi_A,\theta_A)|^2 + |T_{22}^A C_v^{co}(\phi_A,\theta_A)|^2 \\ &\quad + 2|T_{21}^A C_v^{x}(\phi_A,\theta_A) T_{22}^A C_v^{co}(\phi_A,\theta_A)| \\ &\quad \times \cos[\text{angle}\{T_{21}^A C_v^{x}(\phi_A,\theta_A)\} \\ &\quad - \text{angle}\{T_{22}^A C_v^{co}(\phi_A,\theta_A)\}], \\ |C_{tv}^{x}(\phi,\theta)|^2 &= |T_{11}^A C_v^{x}(\phi_A,\theta_A)|^2 + |T_{12}^A C_v^{co}(\phi_A,\theta_A)|^2 \\ &\quad + 2|T_{11}^A C_v^{x}(\phi_A,\theta_A) T_{12}^A C_v^{co}(\phi_A,\theta_A)| \\ &\quad \times \cos[\text{angle}\{T_{11}^A C_v^{x}(\phi_A,\theta_A)\} \\ &\quad - \text{angle}\{T_{12}^A C_v^{co}(\phi_A,\theta_A)\}], \end{aligned} \tag{6}$$

where C can be either T or R. The expressions in (6) illustrate that if the cosine of the phase differences in (6) is negative, the last term reduces the sum and vice versa. Thus, the change in copolar and cross-polar pattern powers is dependent on the phase difference between these patterns. Therefore, tilting an array can decrease or increase the powers of the apparent cross-polar and copolar patterns as well as their ratios. The expression in (2) now reduces to

$$\begin{aligned} \begin{bmatrix} dV_h(m) \\ dV_v(m) \end{bmatrix} &= C\,\mathbf{R}_{TS}\mathbf{S}\mathbf{T}_{TS}\mathbf{e} \\ &= C\begin{bmatrix} R_{th}^{co} & R_{th}^{x} \\ R_{tv}^{x} & R_{tv}^{co} \end{bmatrix}\begin{bmatrix} s_{hh}(m) & 0 \\ 0 & s_{vv}(m) \end{bmatrix} \\ &\quad \times \begin{bmatrix} T_{th}^{co} & T_{tv}^{x} \\ T_{th}^{x} & T_{tv}^{co} \end{bmatrix}\begin{bmatrix} A_h(m)e^{j\alpha_h(m)} \\ A_v(m)e^{j\alpha_v(m)} \end{bmatrix}. \end{aligned} \tag{7}$$

As the beam is electronically steered at θ_0, ϕ_0 (where $90° - \theta_0$ is elevation and ϕ_0 is azimuth) and M pulses are transmitted in that direction, the total received voltage for the mth sample is an integration over θ and ϕ (Fig. 1):

$$
\begin{aligned}
V_{\mathrm{h}}(m) &= \int_{\Omega} dV_{\mathrm{h}}(m)d\Omega \\
&= C\int_{\Omega}\left\{\begin{bmatrix} T_{\mathrm{th}}^{\mathrm{co}}R_{\mathrm{th}}^{\mathrm{co}}A_{h}(m)e^{j\alpha_{\mathrm{h}}(m)}+ \\ T_{\mathrm{tv}}^{\mathrm{x}}R_{\mathrm{th}}^{\mathrm{co}}A_{v}(m)e^{j\alpha_{\mathrm{v}}(m)} \end{bmatrix}s_{\mathrm{hh}}(m)\right. \\
&\quad \left.+\begin{bmatrix} T_{\mathrm{th}}^{\mathrm{x}}R_{\mathrm{th}}^{\mathrm{x}}A_{\mathrm{h}}(m)e^{j\alpha_{\mathrm{h}}(m)}+ \\ T_{\mathrm{tv}}^{\mathrm{co}}R_{\mathrm{th}}^{\mathrm{x}}A_{\mathrm{v}}(m)e^{j\alpha_{\mathrm{v}}(m)} \end{bmatrix}s_{\mathrm{vv}}(m)\right\}d\Omega, \\
V_{\mathrm{v}}(m) &= \int_{\Omega} dV_{\mathrm{v}}(m)d\Omega \\
&= C\int_{\Omega}\left\{\begin{bmatrix} T_{\mathrm{th}}^{\mathrm{co}}R_{\mathrm{tv}}^{\mathrm{x}}A_{\mathrm{h}}(m)e^{j\alpha_{\mathrm{h}}(m)}+ \\ T_{\mathrm{tv}}^{\mathrm{x}}R_{\mathrm{tv}}^{\mathrm{x}}A_{\mathrm{v}}(m)e^{j\alpha_{\mathrm{v}}(m)} \end{bmatrix}s_{\mathrm{hh}}(m)\right. \\
&\quad \left.+\begin{bmatrix} T_{\mathrm{th}}^{\mathrm{x}}R_{\mathrm{tv}}^{\mathrm{co}}A_{\mathrm{v}}(m)e^{j\alpha_{\mathrm{h}}(m)}+ \\ T_{\mathrm{tv}}^{\mathrm{co}}R_{\mathrm{tv}}^{\mathrm{co}}A_{\mathrm{h}}(m)e^{j\alpha_{\mathrm{v}}(m)} \end{bmatrix}s_{\mathrm{vv}}(m)\right\}d\Omega, \qquad (8)
\end{aligned}
$$

where $d\Omega \equiv \sin(\theta)d\theta d\phi$ (integration along range is omitted as it has no bearing on the results. Then, the polarimetric variables can be computed in the STSR mode as

$$
\begin{aligned}
\hat{Z}_{\mathrm{DR}} &= 10\log_{10}\left(\frac{\hat{S}_{\mathrm{h}}}{\hat{S}_{\mathrm{v}}}\right), \\
|\hat{\rho}_{\mathrm{hv}}(0)| &= \frac{|\hat{R}_{\mathrm{hv}}(0)|}{\sqrt{\hat{S}_{\mathrm{h}}\hat{S}_{\mathrm{v}}}}, \\
\hat{\phi}_{\mathrm{DP}} &= \arg[\hat{R}_{\mathrm{hv}}(0)], \qquad (9)
\end{aligned}
$$

where $\hat{S}_{\mathrm{h}}$ and $\hat{S}_{\mathrm{v}}$ are the signal power estimates in the H and V channels, and $\hat{R}_{\mathrm{hv}}(0)$ is the cross-correlation estimate. These are computed from the corrected samples as

$$
\begin{aligned}
\hat{S}_{\mathrm{h}} &= \frac{1}{M}\sum_{m=0}^{M-1}|cV_{\mathrm{h}}(m)|^2, \\
\hat{S}_{\mathrm{v}} &= \frac{1}{M}\sum_{m=0}^{M-1}|cV_{\mathrm{v}}(m)|^2, \\
\hat{R}_{\mathrm{hv}}(0) &= \frac{1}{M}\sum_{m=0}^{M-1}cV_{\mathrm{h}}^{*}(m)cV_{\mathrm{v}}(m), \qquad (10)
\end{aligned}
$$

where

$$
\begin{aligned}
cV_{\mathrm{h}}(m) &= V_{\mathrm{h}}(m)\exp[-j\alpha_{\mathrm{h}}(m)], \\
cV_{\mathrm{v}}(m) &= V_{\mathrm{v}}(m)\exp[-j\alpha_{\mathrm{v}}(m)]\cdot \qquad (11)
\end{aligned}
$$

The ensemble averages of estimates in (8) are given by Eq. (5) in Ivić (2022).

The estimates in (9) are plagued by two types of biases, the copolar and cross-coupling biases. The former are defined as

$$
\begin{aligned}
\mathrm{BIAS}_{\mathrm{CO}}\,\hat{Z}_{\mathrm{DR}} &= 10\log_{10}\left(\frac{\int_{\Omega}|T_{\mathrm{h}}^{\mathrm{co}}R_{\mathrm{h}}^{\mathrm{co}}|^2d\Omega}{\int_{\Omega}|T_{\mathrm{v}}^{\mathrm{co}}R_{\mathrm{v}}^{\mathrm{co}}|^2d\Omega}\right), \\
\mathrm{BIAS}_{\mathrm{CO}}\,\hat{\phi}_{\mathrm{DP}} &= \arg\left[\int_{\Omega}(T_{\mathrm{h}}^{\mathrm{co}}R_{\mathrm{h}}^{\mathrm{co}})^{*}T_{\mathrm{v}}^{\mathrm{co}}R_{\mathrm{v}}^{\mathrm{co}}d\Omega\right], \qquad (12)
\end{aligned}
$$

while the latter are

$$
\begin{aligned}
\mathrm{BIAS}_{X}\,\hat{Z}_{\mathrm{DR}} &= \langle\hat{Z}_{\mathrm{DR}}\rangle - \mathrm{BIAS}_{\mathrm{CO}}\,\hat{Z}_{\mathrm{DR}} - Z_{\mathrm{DR}}, \\
\mathrm{BIAS}_{X}\,|\hat{\rho}_{\mathrm{hv}}(0)| &= \langle|\hat{\rho}_{\mathrm{hv}}(0)|\rangle - |\rho_{\mathrm{hv}}|, \\
\mathrm{BIAS}_{X}\,\hat{\phi}_{\mathrm{DP}} &= \langle\hat{\phi}_{\mathrm{DP}}\rangle - \mathrm{BIAS}_{\mathrm{CO}}\,\hat{\phi}_{\mathrm{DP}} - \phi_{\mathrm{DP}}, \qquad (13)
\end{aligned}
$$

where $\langle\cdot\rangle$ denotes ensemble average. The copolar biases can be corrected in the signal processing stage if the copolar patterns are characterized with sufficient accuracy at and around main beam peaks. Regarding the cross-coupling biases, these can be mitigated using the previously described methods (e.g., the pulse-to-pulse phase coding). The simplest phase shift code [0°, 180°], can be applied in an alternate manner (i.e., the successive train of phase shifts) or a block fashion (e.g., the first half of the pulses is not coded and the phase is shifted by 180° for the rest of the pulses). Then, summing the instantaneous power and cross-correlation estimates (that are computed from single transmission returns) to compute the second-order quantities, as in (10), effectively removes a portion of the cross-polar signals and reduces the cross-coupling effects. An effect of the alternate phase code application is that the part of the cross-coupled signal (that is not removed via averaging instantaneous estimates) appears shifted relative to the copolar signal in the spectral domain (Ivić 2018a). This is conducive to additional cross-coupling bias suppression via filtering of the shifted cross-polar signals in the spectral domain (when the shifted cross-polar and copolar signals are sufficiently separated in spectra). Additional difficulty poses the presence of ground clutter (GC) because the portion of the GC cross-polar signal appears at the edges of the spectra which may complicate its removal. This suggests that the application of phase codes in the block fashion is more appropriate at lower elevations where the presence of GC is more frequent. This is because it prevents the appearance of GC signal at the spectrum edges. This approach, however, prevents the filtering of the cross-coupled signal which particularly mitigates the $|\hat{\rho}_{\mathrm{hv}}(0)|$ bias (Ivić 2022).

In general, the effectiveness of cross-coupling mitigation methods is inversely proportional to the power levels of cross-polar patterns (relative to the power of copolar patterns). This means that if the ratio of cross-polar to copolar pattern powers is too high, the cross-coupling mitigation results in insufficient bias reduction. In such a case, an option is the use of full correction matrices that require precise knowledge of both the antenna copolar and cross-polar patterns (at and around beam peaks) as already discussed. If full correction is used, analysis in Ivić (2018b) suggests that it should be combined with the pulse-to-pulse phase coding because such an approach reduces the correction sensitivity to cross-polar pattern measurement errors. It should be noted that the full correction method presented in Ivić (2018b) operates on second-order quantities which makes it compatible with the pulse-to-pulse phase coding. This is unlike the corrections proposed in Pang et al. (2016) and Fulton and Chappell (2010) which operate on time series. Further, it is logical to assume that the cross-polar pattern characterization relative errors are larger when the measured values are small (e.g., at and around the principal planes), but errors are likely smaller if the measured values are larger

(e.g., at steering angles farther away from the principal planes). This implies that the use of pulse-to-pulse phase coding is preferable to full matrix correction when possible. This presents a motivation to devise approaches that increase the number of electronic steering angles where the cross coupling can be successfully mitigated using methods that do not require the knowledge of cross-polar patterns. In this respect, slight antenna tilt has the potential to either increase or decrease the number of steering angles where cross-coupling bias mitigation is satisfactory. This is because the antenna tilt changes the apparent antenna patterns, which in turn affects the polarimetric performance. For this reason, it is important to evaluate the polarimetric performance of the tilted antenna, using copolar and cross-polar patterns, to determine which tilt (if any) results in positive effects. In the next section, an example of this evaluation is presented using patterns of a real radar measured in the anechoic chamber.

3. Antenna tilt effects

The effects of the antenna tilt are examined using the measured antenna patterns of the Advanced Technology Demonstrator (ATD). It is a full-size, S-band, planar, proof-of-concept PPAR at the National Weather Radar Testbed (NWRT) in Norman, Oklahoma (https://nssl.noaa.gov/tools/radar/atd/), which functions as a testbed for assessing the PPAR technology for weather observations. The antenna consists of 4864 T/R elements organized in 76 panels with 8×8 radiating elements each. On receive, an overlapped subarray (consisting of 8 panels each) approach is employed. It is used to suppress grating lobes outside of the main beam of the subarray pattern (Herd et al. 2005). Also, the subarray outputs are weighted to reduce the receive pattern sidelobes (which also produces a wider main lobe of the receive pattern compared to the transmit pattern). This results in two-way copolar patterns' beamwidths at the broadside of ~1.6°. The size of the antenna is 4 m × 4 m. A movement in azimuth and elevation is possible because the antenna is on a pedestal attached to a rotator platform.

The far-field ATD antenna transmit and receive copolar and cross-polar patterns were measured by the MIT LL and NSSL in the near-field chamber (Conway et al. 2018; Kowalski et al. 2019) prior to installation in Norman. The measurements captured the effects of all passive and active components present at the time of measurement as well as mutual coupling among radiating elements. This also includes measurement instrumentation, which was an open-waveguide probe. Consequently, the probe patterns (provided by the manufacturer) were used for correction during the signal processing stage when the raw measurements were projected into the far-field to create antenna patterns.

The peak power and phase values of all measured patterns (smoothed to reduce the measurement noise) are shown in Figs. 2 and 3. As expected, these indicate that, relative to the corresponding copolar pattern peak powers, the cross-polar pattern peak powers (Figs. 2c,d,g,h) are the smallest in the vicinity of principal planes. Further, the cross-polar patterns on receive exhibit larger power levels than those on transmit. The differences in coupling through active hardware components [described by $\mathbf{T}_H$ and $\mathbf{R}_H$ in (2)] on transmit and receive (e.g., T/R elements) is likely the source of this effect and in this particular case indicate that the cross coupling in the receive hardware path is larger than in the transmit one (likely caused by the H–V "crossover" switch designed into the ATD's T/R module receive path). Further, it is worth noting that the "nonreciprocal" behavior of the transmit and receive pattern peak powers (Fig. 2) is caused by the scan impedance effects on the active T/R module electronics. The phases on transmit (Figs. 3c,d), and receive (Figs. 3g,h) are given relative to the corresponding copolar patterns in H to better exemplify the phase differences, because these affect the cross-coupling biases as indicated in Ivić (2022). An interesting observation is that an approximate variation of cross-polar pattern phases on transmit and receive agrees with that in Bhardwaj and Rahmat-Samii (2014). Given that the majority of radiators, located farther away from the array edges (i.e., the elements located at the array boundaries experience edge effects), in the array behave similarly, the results in Figs. 2 and 3 may be viewed as patterns of a single element located at or in the vicinity of the large array center when only that element is excited and all other elements are terminated with a specified impedance (i.e., embedded element patterns). This is because the extraction of antenna pattern peak values effectively samples summed copolar and cross-polar patterns of all elements in the array (all of which are similar as previously noted) at a measured steering angle.

The ATD antenna patterns, at desired beam-steering angles, are simulated/calculated using the measurement results shown in Figs. 2 and 3, whereby the embedded element patterns are combined with a theoretical array factor (i.e., a directional two-dimensional function that weights the pattern shapes of individual radiators via controlling the relative phases and amplitudes of the microwaves emitted by the antenna elements in the array).This results in the generation of ATD antenna patterns at beam-steering locations not measured in the near-field chamber. Such an approach captures the differences in copolar gain between H and V (as a function of beam-steering angle) channels as well as the cross-coupling effects. However, it does not capture the imperfect beamforming effects such as differences in the main lobe shape between H and V patterns as well as any departures from the theoretical sidelobe levels. But, because the cross-coupling effects on the polarimetric variable estimates, as a result of antenna tilt, are of primary concern here, the so obtained patterns are appropriate for the following evaluation.

Next, the apparent embedded element patterns, relative to the ground, are recomputed for the antenna 5° tilt using the developments in the appendix. The results are presented in Fig. 4. These exemplify the changes in the apparent embedded element patterns as a result of the antenna tilt. As expected, a visual comparison between Fig. 2 and Fig. 4 corroborates that the most significant changes occur to the apparent cross-polar embedded element patterns. In this particular case, the areas of low cross-pol (shown in shades of blue) shift upward at and in the vicinity of the vertical principal plane but curve downward away from zero azimuth. This is

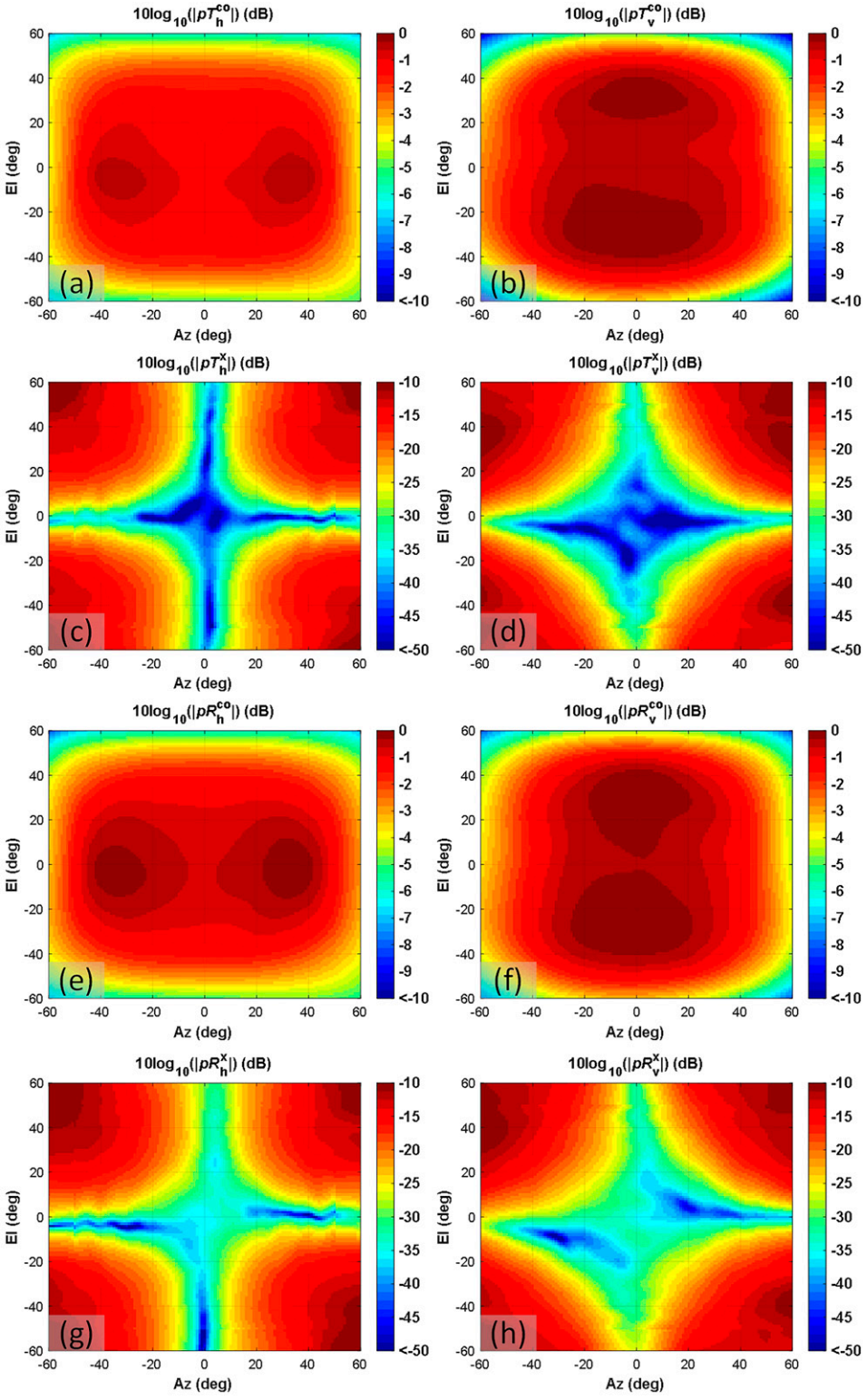

FIG. 2. Peak powers of ATD antenna far-field patterns. Copolar transmit pattern peak powers in (a) H and (b) V. Cross-polar transmit pattern peak powers in (c) H and (d) V. Copolar receive pattern peak powers in (e) H and (f) V. Cross-polar receive pattern peak powers in (g) H and (h) V. On transmit and receive, all power levels are given relative to the maximum power in V. The prefix "*p*," before antenna pattern designation, denotes beam peak.

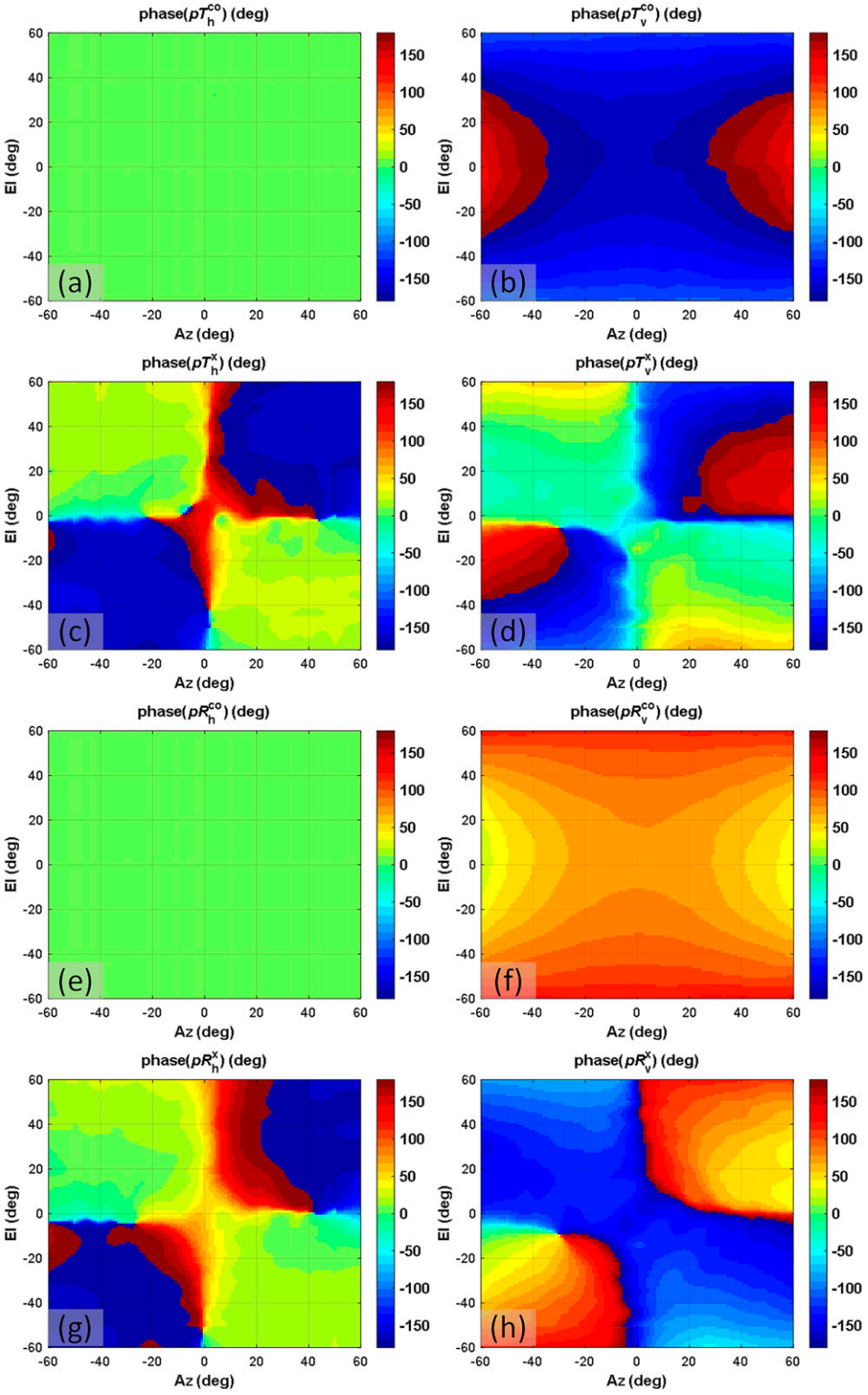

FIG. 3. Peak phases of ATD antenna far-field patterns presented relative to phases of H copolar patterns. Copolar transmit pattern peak phases in (a) H and (b) V. Cross-polar transmit pattern peak phases in (c) H and (d) V. Copolar receive pattern peak phases in (e) H and (f) V. Cross-polar receive pattern peak phases in (g) H and (h) V. The prefix "*p*," before antenna pattern designation, denotes beam peak.

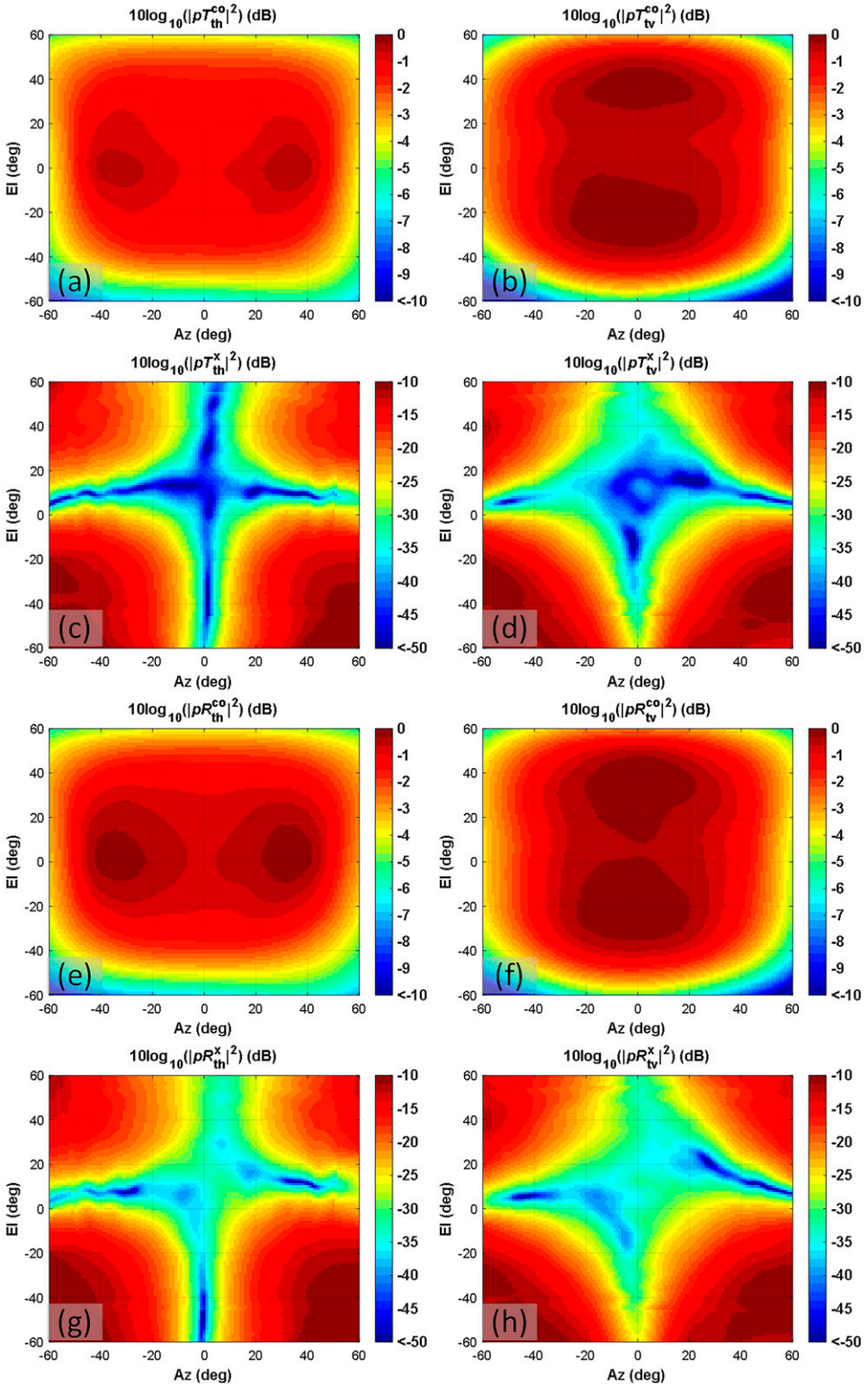

FIG. 4. Peak powers of ATD antenna far-field patterns for the 5° tilt. Copolar transmit pattern peak powers in (a) H and (b) V. Cross-polar transmit pattern peak powers in (c) H and (d) V. Copolar receive pattern peak powers in (e) H and (f) V. Cross-polar receive pattern peak powers in (g) H and (h) V. On transmit and receive, all power levels are given relative to the maximum power in V. The prefix "*p*," before antenna pattern designation, denotes beam peak.

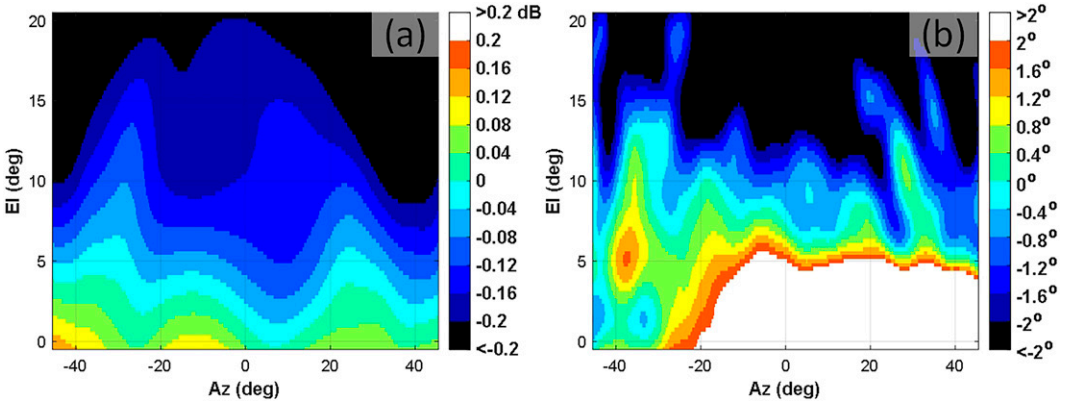

FIG. 5. Differences between copolar biases when the antenna is not tilted and when it is tilted by 5° for (a) $\langle \hat{Z}_{DR} \rangle$ and (b) $\langle \hat{\phi}_{DP} \rangle$.

because the tilt matrix off-diagonal elements are zero along the vertical principal plane but increase gradually at azimuths away from zero (as shown in Fig. A1). The result is that the change in apparent cross-polar patterns is more pronounced at the latter azimuths. Clearly, such rearrangements affect the ensuing copolar and cross-coupling biases in the estimates of polarimetric variables.

The differences between copolar biases in $\langle \hat{Z}_{DR} \rangle$, and $\langle \hat{\phi}_{DP} \rangle$ when the antenna is not tilted and when it is tilted by 5° are in Fig. 5 for a range of beam-steering angles of interest. Note that the $|\hat{\rho}_{hv}(0)|$ biases are omitted as these are not affected by the change in copolar patterns. The results indicate significant differences that exceed the desirable bias limits. These imply that the copolar biases characterized for the antenna perpendicular to the ground need correction if the antenna is tilted. Such correction may be conducted using (5) but requires the knowledge of cross-polar beams for full correction. Alternatively, the correction using (5) may be conducted by neglecting the effects of cross-polar beams (i.e., by setting the values of T_h^x, T_v^x, R_h^x, and R_v^x to zero). The logic behind this is that the changes in the tilted antenna copolar patterns are affected mostly by the product of the known tilt matrix and the copolar pattern values in $\mathbf{T_s}$ and $\mathbf{R_s}$ (4) (because the elements on the main diagonal of $\mathbf{T_s}$ and $\mathbf{R_s}$ are significantly larger than the off-diagonal ones as shown in the appendix).In this particular case, this results in the $\langle \hat{Z}_{DR} \rangle$, and $\langle \hat{\phi}_{DP} \rangle$ bias correction value errors that are within ±0.04 dB, and ±0.6°, respectively (Fig. 6). The other approach is to characterize the copolar biases when the antenna is in the tilt position intended for operational use. The comparison between cross-coupling biases is conducted for the PCSTSR mode, using analytical expressions given in Ivić (2022). The results for the worst-case biases (Ivić 2022) are presented in Fig. 7 for Z_{DR} = 1 dB, and $|\rho_{hv}|$ = 0.98. These indicate a visible change in the biases of polarimetric variable biases. In this particular case, the result is an increase in the cross-coupling biases at lower elevations and the apparent shift of the lower bias areas (particularly in $|\hat{\rho}_{hv}(0)|$, and $\langle \hat{\phi}_{DP} \rangle$ biases) to the upper elevations due to the antenna tilt. This is a consequence of the cross-polar pattern reshaping as shown in Fig. 4 and suggests that a choice of an appropriate antenna tilt may allow for optimization of the polarimetric performance. For the case shown, result in the left column of Fig. 7 suggests that a tilt less than 5° is more appropriate for cross-polar bias mitigation. Also, it implies that the antenna tilt of 10° to 15°, typically used for PAR air-surveillance radars, would not be appropriate

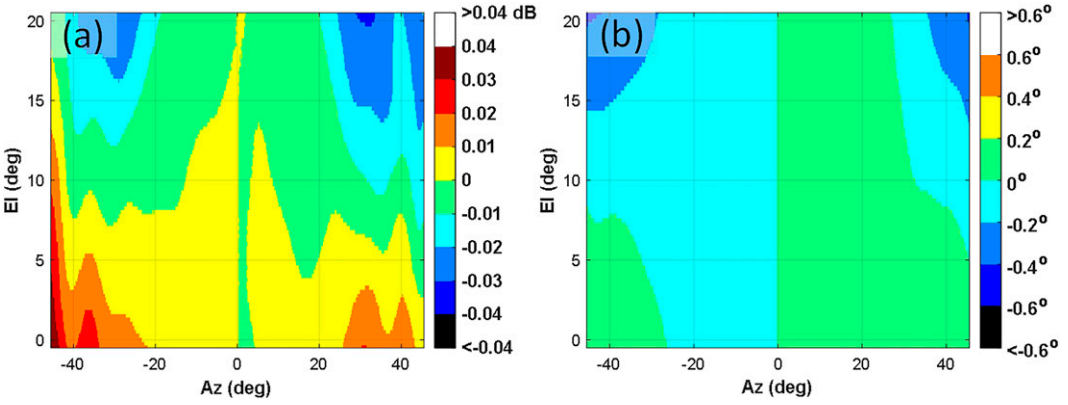

FIG. 6. Errors in the (a) $\langle \hat{Z}_{DR} \rangle$ and (b) $\langle \hat{\phi}_{DP} \rangle$ copolar bias correction as a result of setting the cross-polar values to zero in the case of 5° tilt.

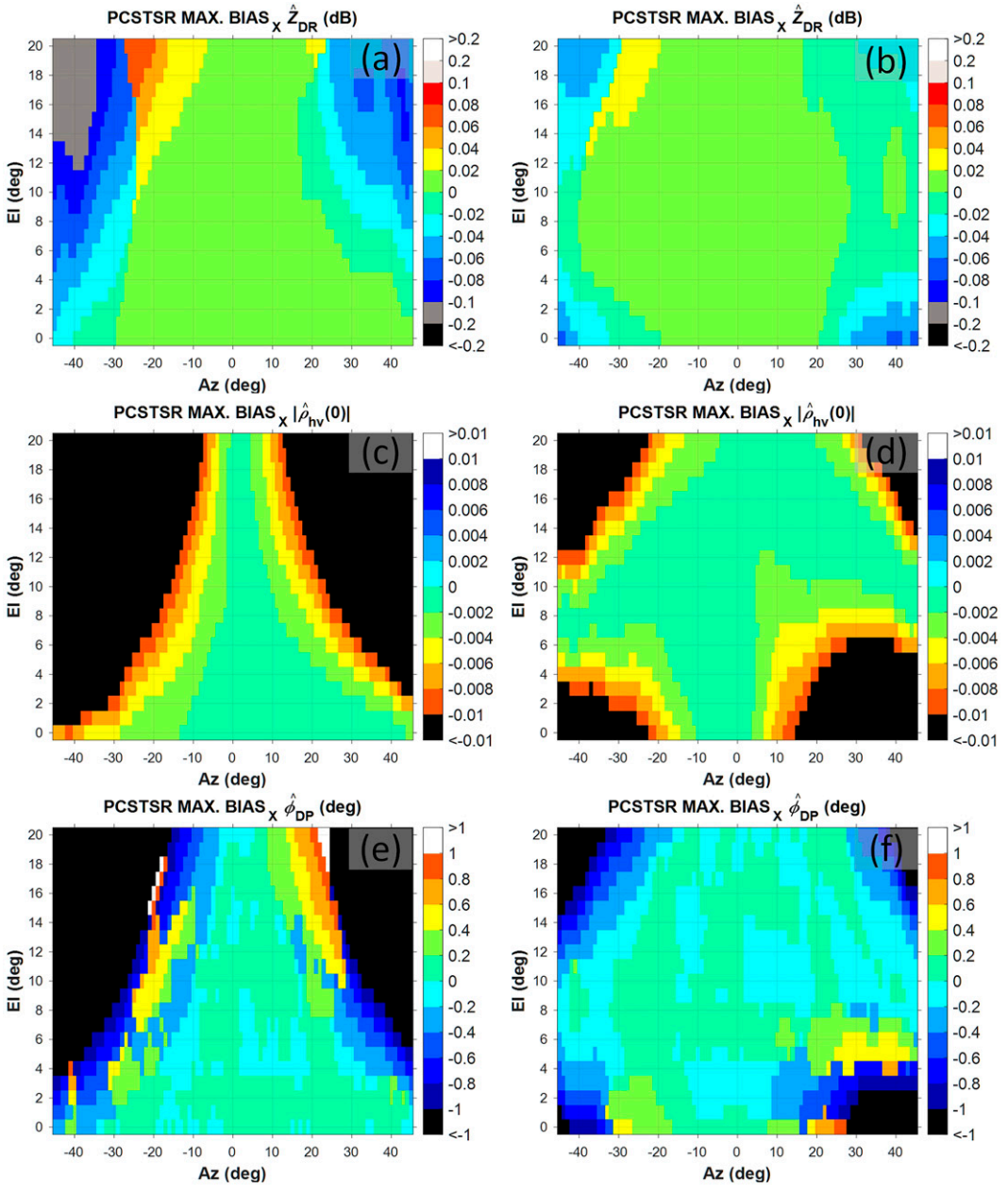

FIG. 7. Cross-coupling biases (left) when the antenna is not tilted and (right) when it is tilted by 5° for (a),(b) $\langle \hat{Z}_{DR} \rangle$, (c),(d) $|\hat{\rho}_{hv}(0)|$, and (e),(f) $\langle \hat{\phi}_{DP} \rangle$.

for weather PPAR because it would cause poor polarimetric performance at lower tilts. In that regard, the cross-coupling biases are shown in Fig. 8 for the 2° tilt. These reveal an increase in the area of acceptable cross-coupling biases at higher elevations and only a small increase in the $|\hat{\rho}_{hv}(0)|$ biases at low elevations (e.g., the lower-right corner in Fig. 8b). In particular, the area of acceptable cross-coupling biases increases from 95.7%, 49.9%, and 70.2% to 99.8%, 69.7%, and 83% for $\langle \hat{Z}_{DR} \rangle$, $|\hat{\rho}_{hv}(0)|$, and $\langle \hat{\phi}_{DP} \rangle$, respectively. This constitutes a small increase of 4.1%, in the case of $\langle \hat{Z}_{DR} \rangle$, but a more significant increase of 19.8%, and 12.8% for $|\hat{\rho}_{hv}(0)|$, and $\langle \hat{\phi}_{DP} \rangle$. In addition, differences between the maximum cross-coupling biases when the antenna is perpendicular to the ground and tilted by 2° is also shown in Fig. 8. These are computed as

$$\text{MAX. BIAS}_X Y \text{ DIFF.} = |\text{MAX. BIAS}_X Y(0^\circ \text{ tilt})| - |\text{MAX. BIAS}_X Y(2^\circ \text{ tilt})|, \quad (14)$$

where Y is $\hat{Z}_{DR}$, $|\hat{\rho}_{hv}(0)|$, or $\hat{\phi}_{DP}$. Visual examination of the differences indicates a general reduction of the cross-coupling biases which has the potential to yield following benefits. The first arises from the fact that the copolar bias corrections are

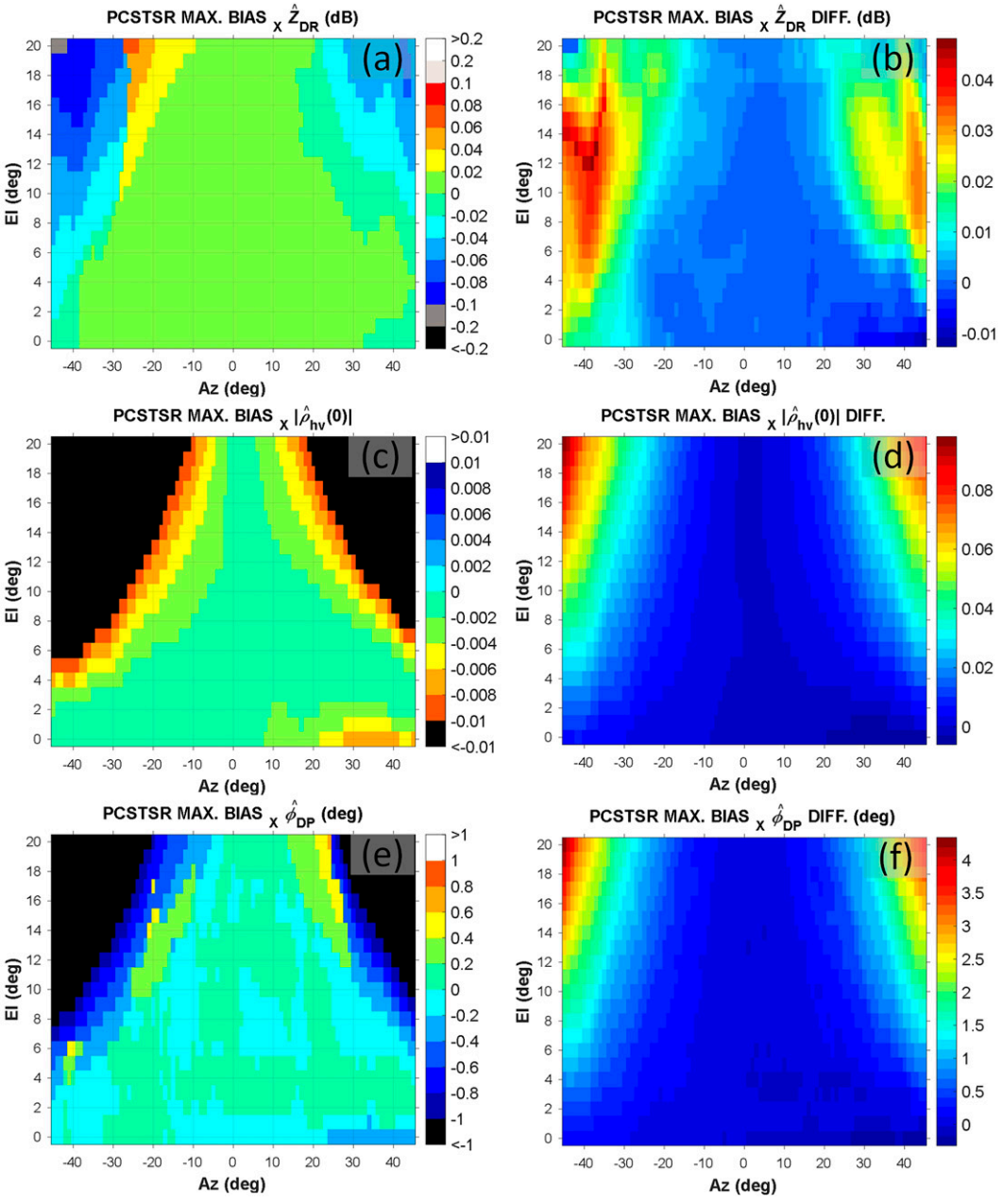

FIG. 8. Cross-coupling biases when the antenna is tilted by 2° for (a) $\langle \hat{Z}_{DR} \rangle$, (c) $|\hat{\rho}_{hv}(0)|$, and (d) $\langle \hat{\phi}_{DP} \rangle$, as well as the cross-coupling bias differences between 0° and 2° tilts for (b) $\langle \hat{Z}_{DR} \rangle$, (d) $|\hat{\rho}_{hv}(0)|$, and (f) $\langle \hat{\phi}_{DP} \rangle$.

inevitably imperfect, due to copolar pattern measurement errors, leading to residual biases which sum with the cross-coupling biases. This summation can be either constructive (if signs of the copolar and cross-coupling biases are the same) or destructive (if signs of the copolar and cross-coupling biases are opposite) resulting in the overall estimation biases. Generally, though, it is logical to assume that as the cross-coupling biases decrease so do the overall estimation biases. Next, a reduction in the cross-coupling biases can potentially improve the efficacy of the cross-coupled signal filtering (Ivić 2022). This implies that the cross-polar performance of a planar PPAR, in this particular case, can be enhanced via a small antenna tilt.

4. Summary and conclusions

In this paper, a description of the antenna tilt effects in PPAR is presented. The main impetus behind the investigation presented herein is to assess whether operating planar PPAR with the array face tilted relative to the ground can result in tangible benefits that improve the accuracy of the radar products. In that regard, a mathematical framework to

compute the apparent copolar and cross-polar antenna patterns relative to the ground (i.e., the antenna patterns in the spherical coordinate system tied to the ground) from the patterns valid when the array is not tilted is developed. To this end, a tilt matrix is derived. It is used to convert radiation patterns from the antenna relative to ground locked coordinate system and vice versa. It is indicated via analytical expressions that the ratio of apparent cross-polar and copolar antenna can either decrease or increase as a result of a particular tilt. Consequently, PPAR antenna tilt can have a positive or negative effect on the overall polarimetric performance whereby such effect is particular to each radar and a chosen antenna tilt. For this reason, it is important to evaluate the antenna tilt effects on an individual radar basis if a PPAR radar antenna in a tilted configuration is to be used operationally. Generally, a chosen antenna tilt will have positive effect if it optimizes the number of electronic steering angles for which the biases of the polarimetric variable estimates are within acceptable limits. As an example, such evaluation is presented in this work using the antenna patterns derived from near-field measurements of the Advanced Technology Demonstrator (ATD) planar PPAR described in the main text.

It is exposed herein that reshaping of the ATD apparent patterns causes an appreciable change of copolar biases in the estimates of differential reflectivity and differential phase. Consequently, if the corrections for these biases are derived for the case when the array is perpendicular to the ground, these need to be recomputed (which can be done using the framework developed herein). Another option is to characterize the antenna beams when the array is in the tilted position intended for operational use. Further, a significant change in the cross-polar patterns, as a result of the tilt, is demonstrated. Investigation reveals that, in the case shown, the areas of lower cross-polar pattern levels (relative to the corresponding copolar patterns) shift toward the upper elevations if the tilt is positive. This reduces cross-coupling biases at these elevations but also may cause unacceptably high degradation of polarimetric variable estimate accuracies, at low elevation steering angles, if the tilt is excessive. In that regard, it is implied that the antenna tilt of 10°–15°, typically used for PAR air-surveillance radars, would not be appropriate for weather PPAR because it would cause poor polarimetric performance at lower tilts. Thus, it is important to choose the optimal antenna tilt based on the mission objectives. For the case shown, it is found that the small tilt of 2° has beneficial effects on the accuracies of polarimetric variable estimates at upper elevations while maintaining the cross-coupling biases at low elevations within acceptable levels. Such tilt is optimal if one antenna tilt position is used for electronically scanning all positions of interest (i.e., ±45° in azimuth and 0°–20° in elevation). Another approach would be to use several discrete tilts whereby each tilt would be used to scan a specific section where polarimetric variable biases are within acceptable limits. This would improve data quality but slightly increase the scan times. To avoid the latter, it may be more advantageous to continuously move the antenna in elevation while scanning. In such a case, electronic steering that is based on the current mechanical antenna position can be used to compensate for antenna motion to maintain beam-pointing accuracy as well as to avoid beam smearing. Apart from improving the polarimetric performance, section scanning using variable antenna elevations may also have beneficial effects in terms of beamwidth as it would reduce the departure of scanning directions from the principal planes. Finally, it should be noted that there are cases when a radar needs to scan at negative elevations (e.g., at mountainous sites). In such a case, a negative antenna tilt may be beneficial.

Acknowledgments. The author would like to thank Dr. Dušan S. Zrnić, who reviewed this manuscript and provided valuable comments that enhanced it. Funding was provided by NOAA/Office of Oceanic and Atmospheric Research under NOAA–University of Oklahoma Cooperative Agreement NA21OAR4320204, U.S. Department of Commerce.

Data availability statement. No datasets were generated or analyzed during the current study.

APPENDIX

Derivation of the Tilt Matrix

To analyze the effects of the antenna tilt, note that each location ϕ, θ, r in spherical coordinates can be expressed in the cartesian system as

$$\begin{aligned} x &= r\sin\theta\cos\phi, \\ y &= r\sin\theta\sin\phi, \\ z &= r\cos\theta\cdot \end{aligned} \tag{A1}$$

If the antenna is tilted by θ_t, each location with coordinates (x, y, z) in the Cartesian coordinate system tied to the ground has the corresponding location (x_A, y_A, z_A) in the Cartesian system tied to the antenna. Given ϕ, θ, r, the location (x_A, y_A, z_A) can be found using the counterclockwise rotation matrix as

$$\begin{aligned} \begin{bmatrix} x_A \\ y_A \\ z_A \end{bmatrix} &= \begin{bmatrix} \cos\theta_t & 0 & \sin\theta_t \\ 0 & 1 & 0 \\ -\sin\theta_t & 0 & \cos\theta_t \end{bmatrix} \begin{bmatrix} x \\ y \\ z \end{bmatrix} \\ &= \begin{bmatrix} r\sin\theta\cos\phi\cos\theta_t + r\cos\theta\sin\theta_t \\ r\sin\theta\sin\phi \\ -r\sin\theta\cos\phi\sin\theta_t + r\cos\theta\cos\theta_t \end{bmatrix}\cdot \end{aligned} \tag{A2}$$

Then, each location ϕ, θ in spherical coordinates tied to the ground has the corresponding location ϕ_A, θ_A in spherical coordinates tied to the antenna as

$$\begin{aligned} \phi_A &= \arctan\left(\frac{y_A}{x_A}\right) \\ &= \arctan\left(\frac{\sin\theta\sin\phi}{\sin\theta\cos\phi\cos\theta_t + \cos\theta\sin\theta_t}\right), \\ \theta_A &= \arccos\left(\frac{z_A}{\sqrt{x_A^2 + y_A^2 + z_A^2}}\right) \\ &= \arccos(-\sin\theta\cos\phi\sin\theta_t + \cos\theta\cos\theta_t). \end{aligned} \tag{A3}$$

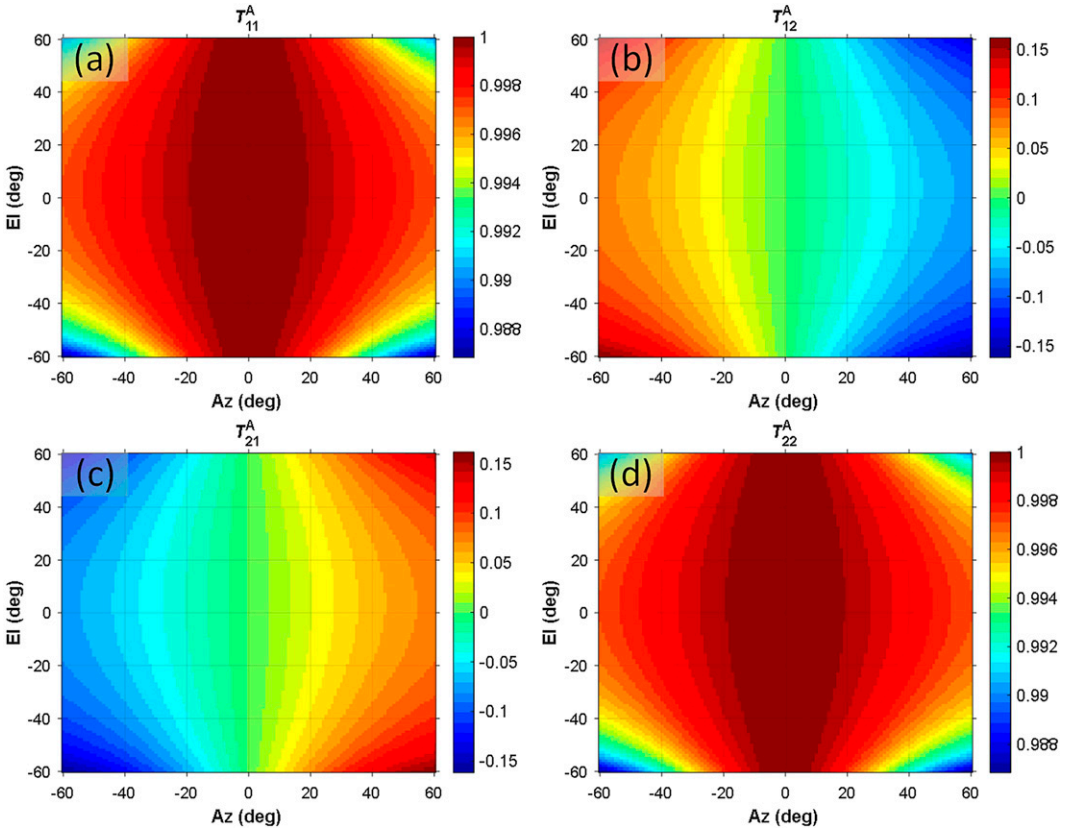

FIG. A1. Values of the tilt matrix elements for 5° tilt. (a) T^{A}_{11}, (b) T^{A}_{12}, (c) T^{A}_{21}, and (d) T^{A}_{22}.

Thus, if desired scan angle is at ϕ_0, θ_0 (in the spherical coordinates tied to the ground) the commanded location to which the tilted array must steer the beam, to point at ϕ_0, θ_0, is found using (A3). Following the same rationale, each location ϕ_A, θ_A in spherical coordinates tied to the antenna has the corresponding location ϕ, θ in spherical coordinates tied to the ground as

$$\phi = \arctan\left(\frac{\sin\theta_A \sin\phi_A}{\sin\theta_A \cos\phi_A \cos\theta_t - \cos\theta_A \sin\theta_t}\right),$$
$$\theta = \arccos(\sin\theta_A \cos\phi_A \sin\theta_t + \cos\theta_A \cos\theta_t). \quad \text{(A4)}$$

The antenna tilt also changes the resultant co- and cross-polar patterns relative to the ground. This can be described by first noting that at each ϕ, θ pattern location the field vectors can be converted from spherical into a Cartesian coordinate system and vice versa as

$$\begin{bmatrix} \mathbf{E}_x(x, y, z) \\ \mathbf{E}_y(x, y, z) \\ \mathbf{E}_z(x, y, z) \end{bmatrix} = \begin{bmatrix} -\sin\phi & \cos\theta\cos\phi \\ \cos\phi & \cos\theta\sin\phi \\ 0 & -\sin\theta \end{bmatrix} \begin{bmatrix} \mathbf{E}_\phi(\phi, \theta) \\ \mathbf{E}_\theta(\phi, \theta) \end{bmatrix},$$

$$\begin{bmatrix} \mathbf{E}_\phi(\phi, \theta) \\ \mathbf{E}_\theta(\phi, \theta) \end{bmatrix} = \begin{bmatrix} -\sin\phi & \cos\phi & 0 \\ \cos\theta\cos\phi & \cos\theta\sin\phi & -\sin\theta \end{bmatrix} \begin{bmatrix} \mathbf{E}_x(x, y, z) \\ \mathbf{E}_y(x, y, z) \\ \mathbf{E}_z(x, y, z) \end{bmatrix}. \quad \text{(A5)}$$

Then, to get the field vectors in the ground Cartesian coordinates from the antenna Cartesian coordinates, the rotation by $-\theta_t$ is applied as

$$\begin{bmatrix} \mathbf{E}_x(x, y, z) \\ \mathbf{E}_y(x, y, z) \\ \mathbf{E}_z(x, y, z) \end{bmatrix} = \begin{bmatrix} \cos\theta_t & 0 & -\sin\theta_t \\ 0 & 1 & 0 \\ \sin\theta_t & 0 & \cos\theta_t \end{bmatrix} \begin{bmatrix} \mathbf{E}^A_x(x_A, y_A, z_A) \\ \mathbf{E}^A_y(x_A, y_A, z_A) \\ \mathbf{E}^A_z(x_A, y_A, z_A) \end{bmatrix}, \quad \text{(A6)}$$

where the vectors on the right and left represent the fields in the antenna and ground-tied coordinates. Using (A5) and (A6), the same can be obtained for the spherical coordinates as

$$\begin{bmatrix} \mathbf{E}_\phi(\phi, \theta) \\ \mathbf{E}_\theta(\phi, \theta) \end{bmatrix} = \begin{bmatrix} -\sin\phi & \cos\phi & 0 \\ \cos\theta\cos\phi & \cos\theta\sin\phi & -\sin\theta \end{bmatrix} \times \begin{bmatrix} \cos\theta_t & 0 & -\sin\theta_t \\ 0 & 1 & 0 \\ \sin\theta_t & 0 & \cos\theta_t \end{bmatrix} \times \begin{bmatrix} -\sin\phi_A & \cos\theta_A\cos\phi_A \\ \cos\phi_A & \cos\theta_A\sin\phi_A \\ 0 & -\sin\theta_A \end{bmatrix} \begin{bmatrix} \mathbf{E}^A_\phi(\phi_A, \theta_A) \\ \mathbf{E}^A_\theta(\phi_A, \theta_A) \end{bmatrix}. \quad \text{(A7)}$$

The expression (A.7) can be reduced to yield the tilt matrix $\mathbf{T}_A$ as

$$\begin{bmatrix} \mathbf{E}_\phi(\phi, \theta) \\ \mathbf{E}_\theta(\phi, \theta) \end{bmatrix} = \begin{bmatrix} T^A_{11} & T^A_{12} \\ T^A_{21} & T^A_{22} \end{bmatrix} \begin{bmatrix} \mathbf{E}^A_\phi(\phi_A, \theta_A) \\ \mathbf{E}^A_\theta(\phi_A, \theta_A) \end{bmatrix}, \quad \text{(A8)}$$

where

$$T_{11}^{A} = \sin\phi \sin\phi_A \cos\theta_t + \cos\phi \cos\phi_A,$$

$$T_{12}^{A} = \cos\phi \cos\theta_A \sin\phi_A - \sin\phi(\cos\theta_A \cos\phi_A \cos\theta_t + \sin\theta_A \sin\theta_t),$$

$$T_{21}^{A} = \cos\theta \sin\phi \cos\phi_A + \sin\phi_A(\sin\theta \sin\theta_t - \cos\theta \cos\phi \cos\theta_t),$$

$$T_{22}^{A} = \cos\theta \cos\phi(\cos\theta_A \cos\phi_A \cos\theta_t + \sin\theta_A \sin\theta_t) + \cos\theta \sin\phi \cos\theta_A \sin\phi_A - \sin\theta(\cos\theta_A \cos\phi_A \sin\theta_t - \sin\theta_A \cos\theta_t) \cdot \quad \text{(A9)}$$

Visual representation of the tilt matrix elements is given in Fig. A1 for 5° tilt. It indicates that the elements on the main diagonal are close to one in the vicinity of the vertical principal plane but gradually decrease at azimuths away from zero. The elements on the off-diagonal, however, are close to zero in the vicinity of the vertical principal plane but gradually increase at azimuths away from zero. This suggests that the apparent antenna patterns increasingly depart from the original ones as beams are steered away from 0° azimuth. This effect is significantly more pronounced in the case of cross-polar patterns. This is because the addition of the small portion of a large copolar pattern [weighted by the off-diagonal elements of the tilt matrix as shown in (5)] to the significantly smaller cross-polar one affects the latter pattern considerably but not vice versa.

REFERENCES

Balakrishnan, N., and D. S. Zrnić, 1990: Use of polarization to characterize precipitation and discriminate large hail. *J. Atmos. Sci.*, **47**, 1525–1540, https://doi.org/10.1175/1520-0469(1990)047<1525:UOPTCP>2.0.CO;2.

Bhardwaj, S., and Y. Rahmat-Samii, 2014: Revisiting the generation of cross-polarization in rectangular patch antennas: A near-field approach. *IEEE Antennas Propag. Mag.*, **56**, 14–38, https://doi.org/10.1109/MAP.2014.6821758.

Bringi, V. N., and V. Chandrasekar, 2001: *Polarimetric Doppler Weather Radar*. Cambridge University Press, 636 pp.

Chandrasekar, V., and N. Bharadwaj, 2009: Orthogonal channel coding for simultaneous co- and cross-polarization measurements. *J. Atmos. Oceanic Technol.*, **26**, 45–56, https://doi.org/10.1175/2008JTECHA1101.1.

Conway, M. D., D. Du Russel, A. Morris, and C. Parry, 2018: Multifunction Phased Array Radar Advanced Technology Demonstrator nearfield test results. *2018 IEEE Radar Conf.*, Oklahoma City, OK, IEEE, 1412–1415, https://doi.org/10.1109/RADAR.2018.8378771.

Crain, G. E., and D. Staiman, 2007: Polarization selection for weather phased array radar. *23rd Conf. on IIPS*, San Antonio, TX, Amer. Meteor. Soc., 7.7, https://ams.confex.com/ams/87ANNUAL/techprogram/paper_118019.htm.

Crum, T. D., and R. L. Alberty, 1993: The WSR-88D and the WSR-88D Operational Support Facility. *Bull. Amer. Meteor. Soc.*, **74**, 1669–1688, https://doi.org/10.1175/1520-0477(1993)074<1669:TWATWO>2.0.CO;2.

Doviak, R. J., and D. S. Zrnić, 1993: *Doppler Radar and Weather Observations*. Academic Press, 562 pp.

——, V. Bringi, A. Ryzhkov, A. Zahrai, and D. Zrnić, 2000: Considerations for polarimetric upgrades to operational WSR-88D radars. *J. Atmos. Oceanic Technol.*, **17**, 257–278, https://doi.org/10.1175/1520-0426(2000)017<0257:CFPUTO>2.0.CO;2.

Fulton, C., and W. J. Chappell, 2010: Calibration of a digital phased array for polarimetric radar. *2010 IEEE MTT-S Int. Microwave Symp.*, Anaheim, CA, IEEE, 161–164, https://doi.org/10.1109/MWSYM.2010.5517964.

——, and Coauthors, 2017: Cylindrical polarimetric phased array radar: Beamforming and calibration for weather applications. *IEEE Trans. Geosci. Remote Sens.*, **55**, 2827–2841, https://doi.org/10.1109/TGRS.2017.2655023.

Galletti, M., D. S. Zrnić, F. Gekat, and P. Goelz, 2014: Eigenvalue signal processing for weather radar polarimetry: Removing the bias induced by antenna coherent cross-channel coupling. *IEEE Trans. Geosci. Remote Sens.*, **52**, 7695–7707, https://doi.org/10.1109/TGRS.2014.2316821.

Heinselman, P. L., and S. M. Torres, 2011: High-temporal-resolution capabilities of the National Weather Radar Testbed Phased-Array Radar. *J. Appl. Meteor. Climatol.*, **50**, 579–593, https://doi.org/10.1175/2010JAMC2588.1.

Herd, J. S., S. M. Duffy, and H. Steyskal, 2005: Design considerations and results for an overlapped subarray radar antenna. *Proc. IEEE Aerospace Conf.*, Big Sky, MT, IEEE, 1087–1092, https://doi.org/10.1109/AERO.2005.1559399.

Illingworth, A., and R. J. Thompson, 2011: Radar bright band correction using the linear depolarization ratio. *Eighth Int. Symp. on Weather Radar and Hydrology*, Exeter, United Kingdom, IAHS, 64–68, http://www.met.reading.ac.uk/radar/publications/LDR.pdf.

Ivić, I. R., 2016: Statistical evaluation of time multiplexing to mitigate differential reflectivity bias due to cross-polar coupling. *J. Atmos. Oceanic Technol.*, **33**, 127–147, https://doi.org/10.1175/JTECH-D-14-00224.1.

——, 2017: Phase code to mitigate the copolar correlation coefficient bias in PPAR weather radar. *IEEE Trans. Geosci. Remote Sens.*, **55**, 2144–2166, https://doi.org/10.1109/TGRS.2016.2637720.

——, 2018a: Effects of phase coding on Doppler spectra in PPAR weather radar. *IEEE Trans. Geosci. Remote Sens.*, **56**, 2043–2065, https://doi.org/10.1109/TGRS.2017.2772962.

——, 2018b: Options for polarimetric variable measurements on the MPAR Advanced Technology Demonstrator. *2018 IEEE Radar Conf.*, Oklahoma City, OK, IEEE, 129–134, https://doi.org/10.1109/RADAR.2018.8378544.

——, 2022: Quantification of polarimetric PAR effects on weather observables in the phase coded STSR mode. *IEEE Trans. Geosci. Remote Sens.*, **60**, 5110022, https://doi.org/10.1109/TGRS.2022.3146358.

——, and R. J. Doviak, 2016: Evaluation of phase coding to mitigate differential reflectivity bias in polarimetric PAR. *IEEE Trans. Geosci. Remote Sens.*, **54**, 431–451, https://doi.org/10.1109/TGRS.2015.2459047.

——, R. Mendoza, D. Schvartzman, S. Torres, and D. Wasielewski, 2021: Preliminary report on polarimetric calibration for the Advanced Technology Demonstrator. NOAA/NSSL Tech. Rep., 34 pp., https://www.nssl.noaa.gov/publications/mpar_reports/Preliminary%20Report%20on%20Polarimetric%20Calibration%20for%20the%20Advanced%20Technology%20Demonstrator.pdf.

Josefsson, L., and P. Persson, 2006: *Conformal Array Antenna Theory and Design*. 1st ed. Wiley–IEEE Press, 512 pp.

Karimkashi, S., and G. Zhang, 2015: Optimizing radiation patterns of a cylindrical polarimetric phased-array radar for

multimissions. *IEEE Trans. Geosci. Remote Sens.*, **53**, 2810–2818, https://doi.org/10.1109/TGRS.2014.2365362.

Kowalski, E., D. Conway, A. Morris, and C. Parry, 2019: Multifunction Phased Array Radar Advanced Technology Demonstrator (MPAR ATD) nearfield testing and fielding. *2019 IEEE Radar Conf.*, Boston, MA, IEEE, https://doi.org/10.1109/RADAR.2019.8835837.

Lei, L., G. Zhang, and R. J. Doviak, 2013: Bias correction for polarimetric phased-array radar with idealized aperture and patch antenna elements. *IEEE Trans. Geosci. Remote Sens.*, **51**, 473–486, https://doi.org/10.1109/TGRS.2012.2198070.

Leifer, M. C., V. Chandrasekar, and E. Perl, 2013: Dual polarized array approaches for MPAR air traffic and weather radar applications. *2013 IEEE Int. Symp. on Phased Array Systems and Technology*, Waltham, MA, IEEE, 485–489, https://doi.org/10.1109/ARRAY.2013.6731876.

Melnikov, V. M., and D. S. Zrnić, 2015: On the alternate transmission mode for polarimetric phased array weather radar. *J. Atmos. Oceanic Technol.*, **32**, 220–233, https://doi.org/10.1175/JTECH-D-13-00176.1.

NOAA/NWS, 2015: NOAA/National Weather Service radar functional requirements. NOAA Doc., 58 pp., https://www.roc.noaa.gov/WSR88D/PublicDocs/NOAA_Radar_Functional_Requirements_Final_Sept%202015.pdf.

Oguchi, T., 1983: Electromagnetic wave propagation and scattering in rain and other hydrometeors. *Proc. IEEE*, **71**, 1029–1078, https://doi.org/10.1109/PROC.1983.12724.

Orzel, K. A., and S. J. Frasier, 2018: Weather observation by an electronically scanned dual-polarization phase-tilt radar. *IEEE Trans. Geosci. Remote Sens.*, **56**, 2722–2734, https://doi.org/10.1109/TGRS.2017.2782480.

Pang, C., P. Hoogeboom, F. Le Chevalier, H. W. J. Russchenberg, J. Dong, T. Wang, and X. Wang, 2016: Polarimetric bias correction of practical planar scanned antennas for meteorological applications. *IEEE Trans. Geosci. Remote Sens.*, **54**, 1488–1504, https://doi.org/10.1109/TGRS.2015.2481610.

Pidre, J. M., M. V. Isasa, and V. Santalla del Río, 2017: Antenna cross-polar requirements for 3-PolD weather radar measurements. *IEEE Trans. Geosci. Remote Sens.*, **55**, 2682–2692, https://doi.org/10.1109/TGRS.2017.2651582.

Richardson, L. M., W. D. Zittel, R. R. Lee, V. M. Melnikov, R. L. Ice, and J. G. Cunningham, 2017: Bragg scatter detection by the WSR-88D. Part II: Assessment of Z_{DR} bias estimation. *J. Atmos. Oceanic Technol.*, **34**, 479–493, https://doi.org/10.1175/JTECH-D-16-0031.1.

Ryzhkov, A. V., and D. S. Zrnić, 2007: Depolarization in ice crystals and its effect on radar polarimetric measurements. *J. Atmos. Oceanic Technol.*, **24**, 1256–1267, https://doi.org/10.1175/JTECH2034.1.

Sachidananda, M., and D. S. Zrnić, 1985: Z_{DR} measurement considerations for a fast scan capability radar. *Radio Sci.*, **20**, 907–922, https://doi.org/10.1029/RS020i004p00907.

——, and ——, 1999: Systematic phase codes for resolving range overlaid signals in a Doppler weather radar. *J. Atmos. Oceanic Technol.*, **16**, 1351–1363, https://doi.org/10.1175/1520-0426(1999)016<1351:SPCFRR>2.0.CO;2.

Schvartzman, D., 2020: Signal processing techniques and concept of operations for polarimetric rotating phased array radar. Ph.D. dissertation, University of Oklahoma, 251 pp., https://hdl.handle.net/11244/326580.

——, S. M. Torres, and T.-Y. Yu, 2021a: Motion-compensated steering: Enhanced azimuthal resolution for polarimetric rotating phased array radar. *IEEE Trans. Geosci. Remote Sens.*, **59**, 10 073–10 093, https://doi.org/10.1109/TGRS.2021.3055033.

——, ——, and ——, 2021b: Distributed beams: Concept of operations for polarimetric rotating phased array radar. *IEEE Trans. Geosci. Remote Sens.*, **59**, 9173–9191, https://doi.org/10.1109/TGRS.2020.3047090.

——, ——, and ——, 2022: Integration of the motion-compensated steering and distributed beams' techniques for polarimetric rotating phased array radar. *IEEE Trans. Geosci. Remote Sens.*, **19**, 3508905, https://doi.org/10.1109/LGRS.2021.3113564.

Siggia, A. D., and R. E. Passarelli, 2004: Gaussian model adaptive processing (GMAP) for improved ground clutter cancelation and moment calculation. *Proc. Third European Conf. on Radar Meteorology*, Visby, Sweden, ERAD, 67–73, http://copernicus.org/erad/2004/online/ERAD04_P_67.pdf.

Sirmans, D., D. Zrnić, and B. Bumgarner, 1976: Extension of maximum unambiguous Doppler velocity by use of two sampling rates. Preprints, *17th Conf. on Radar Meteorology*, Seattle, WA, Amer. Meteor. Soc., 23–28.

Stagliano, J. J., and E. J. Holder, 2010: Mitigation of cross-polar interference in polarimetric weather radar. *26th Conf. on Interactive Information and Processing Systems for Meteorology, Oceanography, and Hydrology*, Atlanta, GA, Amer. Meteor. Soc., 10.B2, https://ams.confex.com/ams/pdfpapers/161798.pdf.

Stapor, D. P., and T. Pratt, 1984: A generalized analysis of dual-polarization radar measurements in rain. *Radio Sci.*, **19**, 90–98, https://doi.org/10.1029/RS019i001p00090.

Torres, S. M., and D. A. Warde, 2014: Ground clutter mitigation for weather radars using the autocorrelation spectral density. *J. Atmos. Oceanic Technol.*, **31**, 2049–2066, https://doi.org/10.1175/JTECH-D-13-00117.1.

——, and Coauthors, 2016: Adaptive-weather-surveillance and multifunction capabilities of the National Weather Radar Testbed phased array radar. *Proc. IEEE*, **104**, 660–672, https://doi.org/10.1109/JPROC.2015.2484288.

Wang, Y., and V. Chandrasekar, 2006: Polarization isolation requirements for linear dual-polarization weather radar in simultaneous transmission mode of operation. *IEEE Trans. Geosci. Remote Sens.*, **44**, 2019–2028, https://doi.org/10.1109/TGRS.2006.872138.

Weber, M., 2019: Meteorological phased array radar research at NOAA's National Severe Storms Laboratory. *2019 IEEE Int. Conf. on Microwaves, Antennas, Communications and Electronic Systems*, Tel Aviv, Israel, IEEE, https://doi.org/10.1109/COMCAS44984.2019.8958067.

——, and Coauthors, 2021: Towards the next generation operational meteorological radar. *Bull. Amer. Meteor. Soc.*, **102**, E1357–E1383, https://doi.org/10.1175/BAMS-D-20-0067.1.

Zhang, G., R. J. Doviak, D. S. Zrnić, J. Crain, D. Staiman, and Y. Al-Rashid, 2009: Phase array radar polarimetry for weather sensing: A theoretical formulation for bias corrections. *IEEE Trans. Geosci. Remote Sens.*, **47**, 3679–3689, https://doi.org/10.1109/TGRS.2009.2029332.

——, ——, ——, R. Palmer, L. Lei, and Y. Al-Rashid, 2011: Polarimetric phased-array radar for weather measurement: A planar or cylindrical configuration. *J. Atmos. Oceanic Technol.*, **28**, 63–73, https://doi.org/10.1175/2010JTECHA1470.1.

Zrnić, D. S., and P. R. Mahapatra, 1985: Two methods of ambiguity resolution in pulsed Doppler weather radars. *IEEE Trans. Aerosp. Electron. Syst.*, **21**, 470–483, https://doi.org/10.1109/TAES.1985.310635.

——, and A. V. Ryzhkov, 1999: Polarimetry for weather surveillance radars. *Bull. Amer. Meteor. Soc.*, **80**, 389–406, https://doi.org/10.1175/1520-0477(1999)080<0389:PFWSR>2.0.CO;2.

——, and Coauthors, 2007: Agile beam phased array radar for weather observations. *Bull. Amer. Meteor. Soc.*, **88**, 1753–1766, https://doi.org/10.1175/BAMS-88-11-1753.

——, R. J. Doviak, G. Zhang, and R. V. Ryzhkov, 2010: Bias in differential reflectivity due to cross coupling through the radiation patterns of polarimetric weather radars. *J. Atmos. Oceanic Technol.*, **27**, 1624–1637, https://doi.org/10.1175/2010JTECHA1350.1.

——, G. Zhang, and R. J. Doviak, 2011: Bias correction and Doppler measurement for polarimetric phased-array radar. *IEEE Trans. Geosci. Remote Sens.*, **49**, 843–853, https://doi.org/10.1109/TGRS.2010.2057436.

——, V. M. Melnikov, and R. J. Doviak, 2012: Issues and challenges for polarimetric measurement of weather with an agile beam phased array radar. NOAA/NSSL Tech. Rep., 119 pp., https://www.nssl.noaa.gov/publications/par_reports/MPAR-WEB_RPT-1_071412-7_May_2_2013_wo_comments.pdf.

——, R. J. Doviak, V. M. Melnikov, and I. R. Ivić, 2014: Signal design to suppress coupling in the polarimetric phased array radar. *J. Atmos. Oceanic Technol.*, **31**, 1063–1077, https://doi.org/10.1175/JTECH-D-13-00037.1.